

Emerging Type-II Superlattices of InAs/InAsSb and InAs/GaSb for Mid-Wavelength Infrared Photodetectors

Dhafer O. Alshahrani,* Manoj Kesaria,* Ezekiel A. Anyebe, V. Srivastava, and Diana L. Huffaker

Mid-wavelength infrared (MWIR) photodetectors (PDs) are highly essential for environmental sensing of hazardous gases, security, defense, and medical applications. Mercury cadmium telluride (MCT) materials have been the most used detector in the MWIR range. However, it is plagued by several challenges including toxicity concerns, a high rate of Auger nonradiative recombination, a large band-to-band (BTB) tunneling current, nonuniformity, and the need for cryogenic cooling. Theoretically, it is predicted that type-II superlattice (T2SL) materials can emerge as an alternative with the potential to outperform the current state-of-the-art MCT PDs due to suppression of Auger recombination associated with bandgap engineering and reduced BTB tunneling current caused by the larger effective mass. Based on this theoretical prediction, it is believed that T2SL have the potential to operate at high temperatures and overcome the size, weight, and power consumption limitations of MCT. Herein, a detailed review of the fundamental material properties of T2SL PDs is provided while providing a comparison of the optical and electrical performances of Ga-free (InAs/InAsSb) and Ga-based (InAs/GaSb) T2SL PDs. Finally, recent advances in IR detection technologies including focal plane arrays and quantum cascade infrared photodetectors are explored.

(MCT/HgCdTe), III–V bulk and type-II superlattice (T2SL) semiconductors is provided.

1.1. II–VI Mercury Cadmium Telluride (MCT)


Mid-wavelength infrared (MWIR) photodetectors (PDs) have been extensively studied for several years and their capabilities well established for applications in environmental gas sensing,^[1] security and defense,^[2] medical diagnostics,^[3] as well as in space and astronomy.^[4] Although several direct bandgap group III–V materials including InAs, InSb, GaSb, and InAsSb are used for MWIR photodetection, mercury cadmium telluride (MCT or called HgCdTe) which is a group II–VI material has been the most used detector owing to its tunable bandgap spanning the mid-wavelength infrared (MWIR: 3–6 μm), long-wavelength infrared (LWIR: 8–14 μm), and very long-wavelength infrared (VLWIR: 14–30 μm) spectral bands. In addition, it has a good

1. Introduction

In this section, a brief introduction about the development of photodetectors based on II–VI mercury cadmium telluride

crystalline quality, strong optical absorption, high quantum efficiency ($\approx 80\%$), and high operating temperature (HOT).^[5] HOT devices normally operate above 77 K which is the main requirement for high-performance IR detectors without the need for cryogenic cooling. The HOT condition is primarily achieved using detectors with a unipolar barrier structure such as *nBn*, which is comprised of a thin *n-type* region, a wide bandgap unipolar barrier layer forming a barrier for electrons but not for holes and an *n-type* absorber region. The *nBn* device structure has two key advantages over a conventional *pin* structure (a photodiode with an undoped, intrinsic region (*i*) sandwiched between the *n*- and *p*-doped regions). 1) At the same operating temperature, the dark current density of the *nBn* detector is lower compared to the *pin* detector. 2) The *nBn* structure can operate at a higher temperature compared to the *pin* structure under the same dark current. However, planar *p-n* MCT detectors have achieved a higher operating temperature with a lower dark current performance compared to the *nBn* structures of III–V semiconductors as exhibited by “Rule 07.”^[6] It has been demonstrated that MCT displays a high device performance and can operate at high temperatures up to $>150\text{ K}$ ^[7–9] due to the long minority carrier lifetime ($\approx 2\text{--}60\text{ }\mu\text{s}$ in the MWIR region).^[10,11] However, MCT suffers from a high rate of Auger nonradiative

D. O. Alshahrani, M. Kesaria, V. Srivastava, D. L. Huffaker^[†]
School of Physics and Astronomy
Cardiff University
The Parade, Cardiff CF24 3AA, UK
E-mail: AlshahraniD@cardiff.ac.uk; KesariaM@cardiff.ac.uk
E. A. Anyebe, D. L. Huffaker,
School of Engineering
Cardiff University
The Parade, Cardiff CF24 3AA, UK

 The ORCID identification number(s) for the author(s) of this article can be found under <https://doi.org/10.1002/adpr.202100094>.

^[†]Present address: Electrical Engineering Department, The University of Texas at Arlington, Arlington 76019, USA

© 2021 The Authors. Advanced Photonics Research published by Wiley-VCH GmbH. This is an open access article under the terms of the Creative Commons Attribution License, which permits use, distribution and reproduction in any medium, provided the original work is properly cited.

DOI: 10.1002/adpr.202100094

recombination, a large band-to-band (BTB) tunneling current which is dominant at high temperatures^[12,13] and mostly requires cryogenic cooling. At low temperatures below 77 K, MCT detectors have shown difficulties and its advantages become less distinct owing to material related challenges including p-type doping, Shockley–Read–Hall (SRH) nonradiative recombination, trap-assisted tunneling (TAT), and surface and interface instabilities due to the weaker ionic bond compared to III–V semiconductors.^[14] In addition, MCT suffers from nonuniformity and has a bandgap with high compositional uniformity. From the environmental perspective, MCT contains harmful components which can impact the environment, as a result, they are mostly limited to applications in the military.

1.2. Bulk III–V Semiconductors

InSb material system is a III–V binary semiconductor that is well matched to the MWIR spectral transmission window. Indeed, the majority of MWIR detectors are made of InSb material operating at 77 K with focal plane array (FPA) formats. InSb detectors offer a high quantum efficiency combined with excellent uniformity and high pixel operability.^[15–17] However, the main limiting factor for InSb materials is the low operating temperature (≈ 80 – 100 K) which hampers its application for uncooled infrared imaging systems.^[18] InAsSb ternary alloy is another III–V semiconductor material that can be also used for MWIR detection applications with demonstrated good device performance. For example, Deng et al.^[19,20] have recently fabricated MWIR high operating temperature (HOT) FPAs InAsSb XBn bulk which can operate at 150 K. Klipstein et al.^[21–23] demonstrated MWIR HOT InAsSb XBn single-pixel detectors and FPAs which can operate at 150 K. Soibel et al.^[24] fabricated MWIR InAsSb nBn detector with potential for temperature operation. The bulk InAsSb material can be also tailored from MWIR to LWIR spectral bands with different Sb composition, however, the main challenge is the lack of a suitable lattice matched substrate. InAsSb bulk also suffers from a high tunneling current which is due to the lower effective mass that is dependent on the bandgap energy. Consequently, there is a quest for alternative materials to replace the current MCT and III–V bulk materials.

1.3. III–V Semiconductors Type-II Superlattice

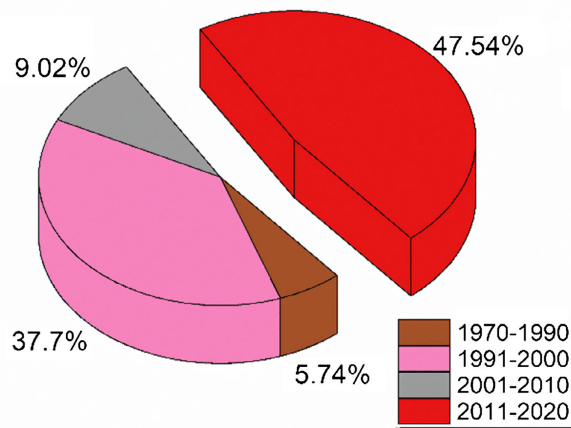
Type-II superlattice (T2SL) materials have emerged as promising alternatives to MCT detectors. Ga-based (InAs/GaSb) and Ga-free (InAs/InAsSb) T2SL detectors are particularly promising with enormous potential to outperform the current state-of-the-art MCT due to favorable detector properties which differ significantly from bulk semiconductors including reduced BTB tunneling current resulting from larger electron effective mass and mobility,^[25] broad wavelength spectrum spanning from the MWIR to VLWIR regime,^[5] and suppressed nonradiative Auger recombination,^[26–28] due to flexibility of bandgap engineering and the spatial separation of electrons and holes in the T2SL enabling HOT device operation. Although it has been theoretically predicted that the Auger recombination lifetime of Ga-based InAs/GaSb SL is suppressed by several orders of magnitude compared to bulk MCT with similar bandgap energy,^[29]

this is yet to be experimentally demonstrated. The T2SL materials also possess several intrinsic advantages including excellent material uniformity over large areas, structural stability owing to strong chemical bonding,^[30,31] low fabrication cost,^[32] availability of a lattice-matched substrate,^[32] and mature material growth.^[32] Consequently, T2SL single-pixel PDs and emitters have been the foci of attention ever since the first theoretical proposals were reported in the early 1970s and late 1980s.^[33,34] The first theoretical investigations of superlattices were reported by Esaki and Tsu^[33] and Sai-Halasz et al.^[35] in the 1970s, followed by an experimental demonstration of InAs/GaSb T2SL by Sakaki et al.^[36] The Ga-based material system was then proposed for use in IR detection by Smith and Mailhot.^[34] InGaSb/InAs SL has also been widely explored for IR photodetector applications. This SL structure benefits also from the adjustability of wavelength and suppression of Auger recombination due to the large band offsets. However, its application has been hampered by major extrinsic materials issues, namely, a high density of SRH centers.^[37] The InGaSb/InAs SL structures still require further enhancement in photodetector performance which is likely due to the limitation of minority carrier lifetime. In addition, a large number of defects have been identified in these structures owing to interface intermixing which limit their performance. In contrast, the initial demonstration of Ga-free InAs/InAsSb SL was in 1994 by Biefeld et al.^[38] using an InAs/InAsSb strained-layer SL with low antimony (Sb) content (below 20%), grown by metal-organic chemical vapor deposition (MOCVD) on InAs substrates and by molecular beam epitaxy (MBE) on GaAs substrates.^[39] In 1995, the first Ga-free InAs/InAsSb SL MWIR lasers with the continuous-wave operation were reported by Zhang which demonstrates their capabilities for use in IR emitters.^[40] In the last two decades, significant progress has been made in the design and performance of MWIR T2SL for IR photodetection.

An overview of research interests in Ga-free and Ga-based T2SL in the last five decades is provided in **Figure 1**. This shows that there has been increasing research interest in T2SL since the 1970s, although, there were fewer research publications focused on Ga-free SL ($\approx 6\%$) when compared to Ga-based SL ($\approx 11\%$). The number of research publications on Ga-free SL between 1990 and 2000 significantly increased by $\approx 38\%$ as against Ga-based SL ($\approx 19\%$). Conversely, between 2001 and 2010, significant advancements were made in the development of SL detectors with greater emphasis on Ga-based SL ($\approx 31.5\%$). Over the past decade, it is evident that there are more research publications focused on Ga-free T2SL (47.5%) compared to their Ga-based counterparts (38.7%). The use of each SL material presents certain merits and demerits. **Table 1** shows the advantages and disadvantages of Ga-free and Ga-based T2SL PDs.

Given the importance of these two emerging and highly promising T2SL materials, there is an urgent need for a detailed review comparing the properties and performance of these materials to enable easy selection of an appropriate T2SL material depending on the most important figure of merit required for the application. In addition, an update on recent progress made in the development of these two emerging T2SL materials is highly essential. While there are numerous reviews on the history of infrared detectors and the performance of alternative materials to HgCdTe,^[14,25,32,41,42] there is a dearth of a detailed comparative review of Ga-based and Ga-free T2SL photodetector technologies.

(a) Research Publications in Ga-free InAs/InAsSb SL



(b) Research Publications in Ga-based InAs/GaSb SL

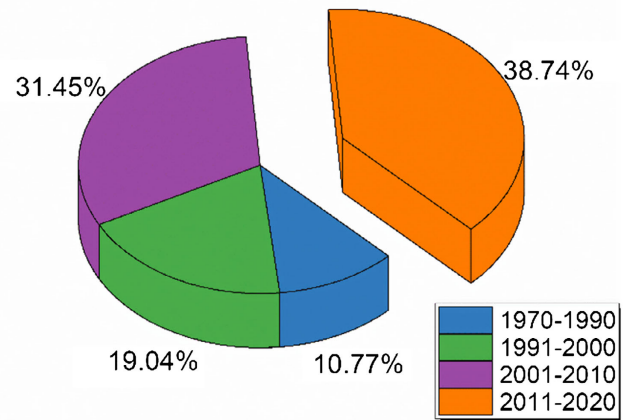


Figure 1. An overview of research publications (in percentage) for both Ga-free InAs/InAsSb a) and Ga-based InAs/GaSb SL b) over the last five decades. Source: Web of Science search using “InAs/GaSb and InAs/InAsSb Type-II Superlattices” in titles, subjects, abstracts, and keywords.

Table 1. A summary of the advantages and disadvantages of InAs/InAsSb and InAs/GaSb SL detectors, where MC is minority carrier and QE is the quantum efficiency.

Material system	Advantages	References	Disadvantages	References
InAs/InAsSb SL	Longer MC lifetime in the MWIR region ($\approx 1.8\text{--}9\text{ }\mu\text{s}$ at 77 K)	[44,45]	Weaker optical absorption coefficient especially at longer wavelengths leading to lower QE	[48–50]
	Less complicated growth sequence as only one shutter needs to be controlled	[14,46]	More challenging vertical hole transport at longer wavelengths	[50–52]
	Better defect tolerance since defects are localized above the conduction band edge	[47]	Smaller conduction and valence band offsets resulting in higher tunneling current rate at HOT	[14]
			Strong dependence of QE on the carrier diffusion length at longer wavelengths; shorter diffusion length leads to lower QE	[48,53]
InAs/GaSb SL	Stronger optical absorption coefficient	[48,56]	Antimony (Sb) segregation issues at the InAs/InAsSb SL interfaces	[54,55]
	Larger conduction and valence band offsets resulting in less tunneling current	[14]	Shorter MC lifetime in the MWIR region (≈ 0.140 to $0.80\text{ }\mu\text{s}$ at 77 K)	[58,59]
	Larger cut-off wavelengths range can be tailored to cover the SWIR to VLWIR spectral bands	[57]	More challenging to grow since four shutters need to be controlled (In, As, Ga, and Sb)	[60,61]
			More sensitive to elemental intermixing at the InAs/GaSb SL interfaces	[62]
			Limited by SRH due to the presence of Ga-element in the GaSb layer	

Recently, Rogalski et al.^[43] have published a review work with a section focusing on the characteristics of SL and barrier PDs. In this article, the fundamental material properties, as well as the optical and electrical performances of the two emerging Ga-based (InAs/GaSb) and Ga-free (InAs/InAsSb) T2SL MWIR photodetector technologies, are comprehensively compared. Recent advances made in the device designs and performance of these detectors are also provided.

2. Fundamental Material Properties of the type-II Superlattice

In this section, the fundamental material properties of the T2SL including bandgap energy and band structures, minority carrier lifetimes, and absorption coefficients are discussed in detail. In addition, materials growth section of Ga-free InAs/InAsSb and Ga-based InAs/GaSb T2SL is presented.

2.1. Bandgap Energy and Band Structure of T2SL

The bandgap energy of different semiconductor materials including InAs, GaSb, AlSb, and InSb is shown in **Figure 2**. Among all III–V semiconductor materials, the InAs_{1–x}Sb_x bulk material system possesses the narrowest bandgap of $\approx 0.1\text{ eV}$ (Sb composition of 60%) at room temperature.^[63] However, bulk materials of InAsSb suffer from a high rate of Auger nonradiative recombination and InAsSb with high Sb composition has no available lattice-matched substrate resulting in high rates of threading dislocations and dark currents. Alternatively, material systems such as strained-layer superlattice are being explored owing to increased wavelength while preserving a lattice-matched substrate and mitigating the emergence of threading dislocations. A superlattice is defined as a one-dimensional (1D) periodic structure which consists of two or more alternating layers. The thicknesses of these layers are commonly thin, of the order

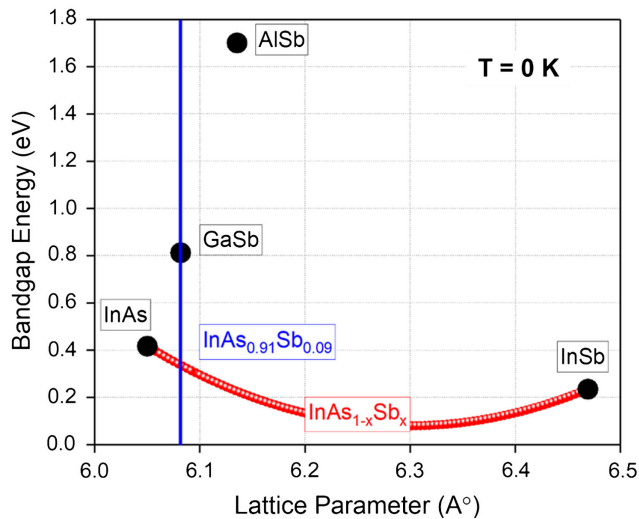


Figure 2. Bandgap energy as a function of lattice constant for several semiconductor materials at 0 K. The red line shows the possibility of forming the lowest bandgap energy by selecting a proper Sb composition in the InAs/InAs_{1-x}Sb_x T2SL.

of 5–20 atomic monolayers (MLs) each. The advantage of utilizing the superlattice structure is that strained layers are introduced leading to bandgap energy minimization and tuning from the MWIR to VLWIR spectral bands.^[64,65] In addition, the formation of strained layers results in a break of the degeneracy of heavy hole (HH) and light hole (LH) in the valence band which leads to suppression of nonradiative Auger recombination processes which is dominant in the bulk materials.^[26–28] As a result of these interesting fundamental properties of SL materials, there has been a flurry of research activities focused on the design and fabrication of single element and FPA detectors.

Figure 3 shows different possibilities of the band structure alignments between InAs, InSb, GaSb, and AlSb. The formation of type-II heterojunction (also called broken gap) is noticed

between the InAs and GaSb and attributed to variations of conduction and valence band offsets (ΔE_C and ΔE_V) as well as the electron affinities. As can be seen, the conduction band of InAs is at a lower energy level than the valence band of GaSb which leads to spatially separating electrons in the conduction band (C_B) of InAs layer and holes in the valence band (V_B) of GaSb layer. Another possibility of heterojunction band alignment is the junction formed between GaSb and AlSb which is called type-I heterojunction. In this case, the smaller bandgap material (GaSb) is sandwiched between two larger bandgap materials (AlSb). However, both carriers of electrons and holes are here confined to each respective layer.

The most crucial property of T2SL is the possibility of bandgap engineering. By varying the Sb composition in the InAsSb alloy of InAs/InAsSb T2SL and layer thicknesses of barriers and wells, the specific wavelength can be tuned. Moreover, the electron effective mass (m_e) is independent of the bandgap energy, compared to bulk semiconductor materials, which leads to lower mobility, and thus; a lower tunneling current.^[25,66] **Figure 4** shows the band structure profile of both T2SL. It can be seen that the ΔE_C and ΔE_V for the Ga-based SL are significantly larger than that of the InAsSb layer in the Ga-free SL.^[67] Note that, the effective bandgap energy of the SL is defined as the difference of the optical transitions from the first electron miniband in the conduction band level to the first heavy hole miniband in the valence band level.

2.2. Minority Carrier Lifetime

The minority carrier (MC) lifetime is a crucial optical characteristic for the SL material which is considered as a key parameter to identify the performance of IR PDs. The MC lifetime contributes directly to the dark current, the detectivity and operating temperature of T2SL detectors and it is dependent on the diffusion length which is described by

$$L = \sqrt{D\tau} \quad (1)$$

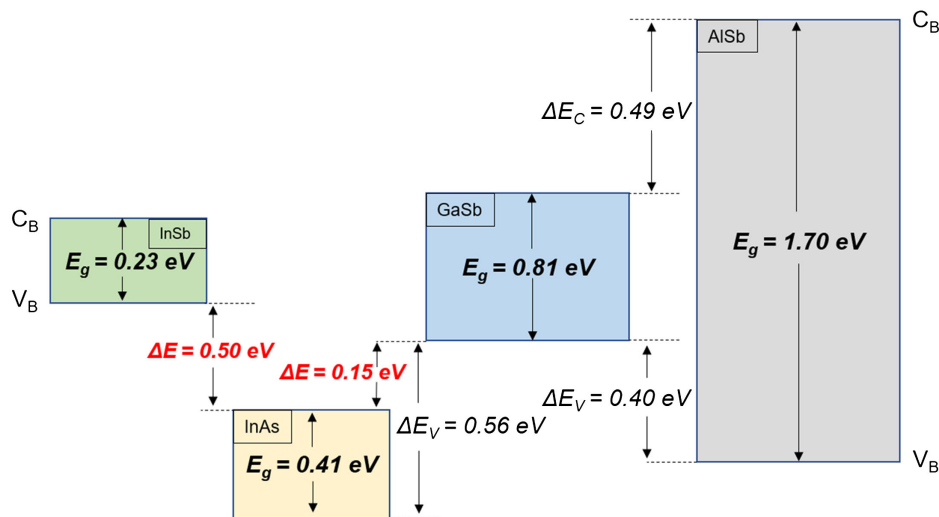


Figure 3. Band structure alignment of InAs/InSb, InAs/GaSb, and GaSb/AlSb at 0 K.

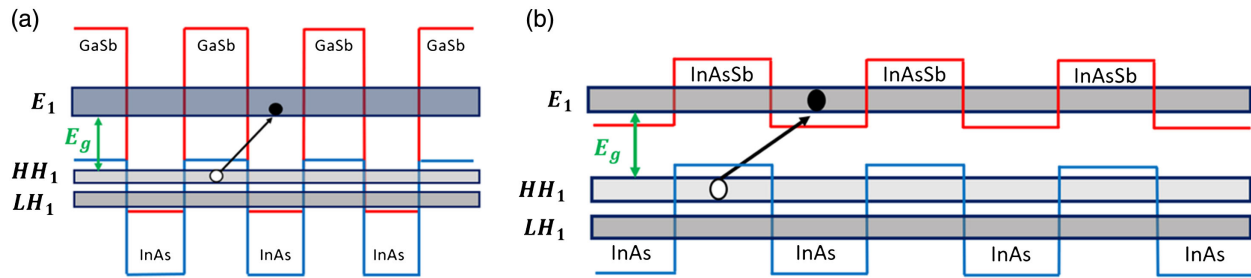


Figure 4. Band structure alignments for a) Ga-based InAs/GaSb and b) Ga-free InAs/InAsSb T2SL. The effective bandgap energy of the SL (highlighted in green) is calculated as the difference between the first electron miniband in the conduction band to the first heavy hole miniband in the valence band.

where L is the diffusion length of the minority carrier, D is the diffusion coefficient, and τ is the minority carrier lifetime. The influence of MC lifetime and diffusion length on the T2SL detector performance is discussed in Section 3.1. Several recombination processes can contribute to the MC lifetime in the T2SL. These are radiative and nonradiative Auger or SRH recombination. In a direct bandgap semiconductor material, radiative recombination takes place when an electron from the conduction band recombines with a hole in the valence band and this process leads to producing a photon (light). In contrast, nonradiative recombination occurs when the recombination of electrons and holes does not lead to photon generation, but alternatively, the produced energy is converted into phonons. Each of these recombination processes has its lifetime (τ) and depends on temperature. The overall lifetime can be expressed as follows

$$\frac{1}{\tau} = \frac{1}{\tau_{\text{Rad}}} + \frac{1}{\tau_{\text{Aug}}} + \frac{1}{\tau_{\text{SRH}}} \quad (2)$$

where τ_{Rad} , τ_{Aug} , and τ_{SRH} are the corresponding radiative, Auger, and Shockley–Read–Hall lifetimes, respectively. The MC lifetime temperature-dependent measurement is a useful technique to identify the dominant recombination mechanism.^[68] In 2013, a study measured the MC lifetimes of Ga-free SL at temperatures between 77 and 250 K.^[44] It was shown that the radiative recombination mechanism was dominant over the temperatures range between 77 and 200 K with a corresponding increase in MC lifetime from 1.8 to 2.8 μs , whereas nonradiative Auger recombination behavior was dominant at higher temperatures above 200 K which limited lifetime. It was demonstrated that the Auger recombination processes can be suppressed by using the T2SL with a further modification in the electronic band structure by adjusting the layer thickness, composition, and strain. This helps to treat the issue associated with the large splitting of HH and LH in the valence band which contributes to increasing the rate of Auger recombination due to the intersubband transition. It was reported that the Auger recombination rate of MWIR Ga-free T2SL is an order of magnitude lower compared to the MCT material system.^[69] BTB radiative and non-radiative Auger recombination rates can be identified only by the intrinsic properties of the material such as absorption spectrum, band structure, and carrier densities. In contrast, the SRH recombination process does not occur in a perfectly pure material. It usually occurs owing to the intentional or unintentional introduction of dopants to the semiconductor materials so that the recombination can happen through defects (trap levels in

the bandgap of the material). These defects are originally formed during the growth procedure owing to the formation of strain, impurities, or dislocations in the structure.

Significantly longer MC lifetimes (10 μs at 80 K^[70]) have been realized in the MWIR range by Ga-free InAs/InAsSb T2SL in comparison to Ga-based InAs/GaSb T2SL (100 ns at 110 K^[71]).^[44,45,70–72] This is attributed to the presence of Ga-element in the InAs/GaSb contributing to the formation of native defects during growth which is deleterious to device performance.^[62] A study by Lin et al.^[73] conducted the MC lifetime temperature-dependence and PL spectra measurements of MWIR Ga-free InAs/InAsSb SL. A long MC lifetime of 12.8 μs at 15 K was observed in the MWIR Ga-free SL owing to carrier localization effect and a decrease in MC was observed with increasing temperature. Another study^[74] indicated that the influence of carrier localization is due to variations in the InAsSb compositions, interfaces, and thicknesses of InAs and InAsSb. It was pointed out that the effect of interface disorder and carrier localization become more distinct in SL with shorter periods.^[73] In the case of Ga-based SL, it was found that MC lifetime decreases in the low-temperature range from 11 to 100 K which could be also attributed to the carrier localization effect, but it is also strongly limited by the impact of SRH recombination centers.^[59,75] For a detailed discussion about the effect of carrier localization and interface disorder on minority carrier lifetime and device performance, the reader is guided to the following references.^[42,73,74] A study by Aytac et al.^[70,72] demonstrated that the MC lifetime of Ga-free InAs/InAsSb SL can be increased by reducing the layer thickness and increasing Sb composition in the InAs_{1-x}Sb_x alloy. Several nondoped MWIR Ga-free T2SL samples were designed to have the same wavelengths of 5.2 μm at 77 K, but with some variations in the layer thicknesses and Sb compositions. It was found that when the Sb compositions are increased and layer thicknesses are reduced, the MC lifetimes increase from 4.5 to 10 μs . This was attributed to the decrease in SRH recombination rates which leads to enhancing the MC lifetimes.

Figure 5 summarizes the reported minority carrier lifetimes over the last 15 years for different semiconductor materials at a low temperature of 77 K in the MWIR regime. As can be seen, although the MCT material possesses the longest MC lifetime of $\approx 59 \mu\text{s}$, the Ga-free InAs/InAsSb SL has comparable lifetimes. This is followed by InAs, InSb, and InAsSb with significantly higher MC lifetimes compared to the GaSb material. The Ga-based InAs/GaSb SL consistently has the lowest MC lifetimes of typically $\leq 0.1 \mu\text{s}$ at 77 K. In spite of the significantly higher

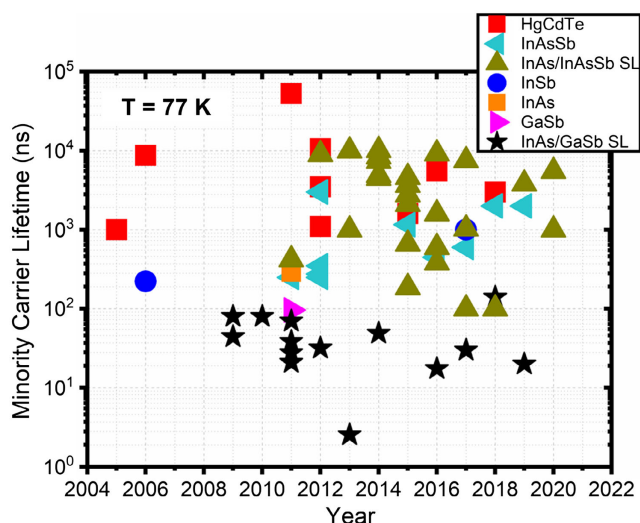


Figure 5. A summary of the most reported data of minority carrier lifetimes at 77 K for Ga-free SL_n [42,44,45,70,76–83] Ga-based SL_n [58,62,71,84–88] HgCdTe/MCT_n [10,11,42,76,89,90] and other binary and ternary III–V material systems. [45,62,77,91–96]

MC lifetime, MWIR InAs/InAsSb SL PDs still demonstrate inferior performance to that state-of-the-art MCT devices due to the presence of more SRH recombination active centers.

2.3. Materials Growth of InAs/GaSb and InAs/InAsSb T2SL

The InAs/InAsSb T2SL has several advantages over the more researched InAs/GaSb T2SL. The Ga-free InAs/InAsSb T2SL is generally easier to grow, has a longer minority carrier lifetime, and it is more tolerant to defects. **Figure 6** compares the conventional MBE shutter sequence growth used for both a) Ga-based InAs/GaSb and b) Ga-free InAs/InAsSb T2SL. In principle, the growth of InAs/InAsSb T2SL involves only turning on and off the Sb shutter, while the In and As shutters remain open during the growth. Conversely, the growth of InAs/GaSb requires the use of four shutters (In, As, Ga, and Sb) which makes it more challenging to obtain sharp interfaces, [60,61,97–99] thus a

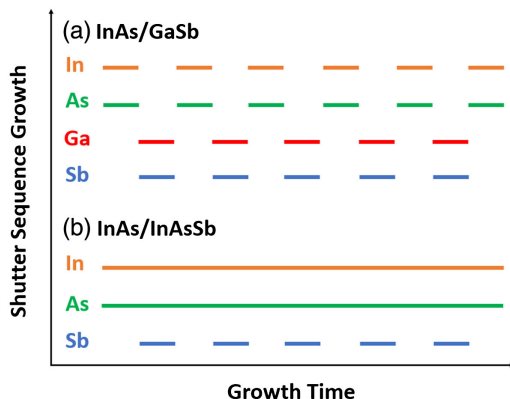


Figure 6. A conventional shutter sequence during materials growth of a) InAs/GaSb and b) InAs/InAsSb T2SL.

complicated interfacial (IF) layer sequence is required to resolve the issue. Note that InAs has a smaller lattice parameter compared to GaSb which results in the formation of defects due to tensile strain. This can be overcome by controlling the interfacial region between the InAs and GaSb layers which can lead to a strain-compensated SL layer with a high structural and optical quality of materials grown. This is mainly dependent on the shutter sequence technique used during the growth, where an InSb layer “InSb-like” IF, a GaAs layer “GaAs-like” IF or a combination of InAs and GaSb leading to ternary/quaternary “mixed-like” IF can be formed. Therefore, when an InSb IF layer is inserted at the SL interfaces of InAs and GaSb layers, the tensile strain in the InAs layers can be compensated by the compressive strain in the InSb layers. Different techniques have already been demonstrated to enhance the optical, structural, and device performances in which the InSb IF layer is inserted between each interface of the SL. One of these is Sb-As exchange shutters technique where each SL layer of InAs is exposed to Sb soak for few seconds. [100,101] The other technique involves the insertion of an intentional InSb layer at the SL interfaces either by using a conventional MBE growth procedure (the In and Sb shutters are asynchronously opened) [102] or by migration enhanced epitaxy (MEE) (the In and Sb shutters are synchronously opened). [103]

The interfacial issue is the main obstacle for high-quality growth of InAs/GaSb T2SL which has a critical impact on the structural, optical, and device performance. Consequently, the intentional incorporations of interfacial layers are currently being employed to circumvent this challenge at the InAs/GaSb interfaces including GaAs-like, [104–107] InSb-like, [108–112] and ternary/quaternary mixed-like IFs [113] with demonstrated evidence of enhanced device performance. Much evidence has proved that InAs/GaSb T2SL with GaAs-like IFs performs poorly for IR detection [104,105] and it is generally avoided. So far, several research groups have tried to investigate the effect of interfacial growth control on the structural, optical, and electrical performances. Huang et al. [106,107] grew an InAs/GaSb T2SL on an InAs substrate incorporating a GaAs IF layer at the SL interface by MOCVD. Deng et al. [108] have also tried inserting a 1 ML of an InSb IF layer between InAs/GaSb T2SL grown on a Si substrate to attain a strain-balanced condition. Jie et al. [109] also studied the influence of inserting InSb IF layers at the SL interfaces grown on GaSb and GaAs substrates. Jie et al. [113] also demonstrated growth of mixed-like IFs (i.e., GaInAsSb-like IFs) and found that the PL spectra of SL with mixed-like IFs showed a stronger PL intensity and narrower full width at half maximum compared to InSb-like IFs, however, the mixed-like IFs appeared to be more sensitive to growth temperature than that with InSb-like IFs as demonstrated by X-ray diffraction (XRD) and atomic force microscope (AFM) measurements. More recently, Huang et al. [110] have performed growth of LWIR InAs/GaSb T2SL using a modified migration enhanced epitaxial (MMEE) growth technique to insert an additional Sb soak and InSb IF layers at the second SL interfaces. In this method, a growth stop and an additional Sb soak were performed at the second IFs between InAs layer growth and In deposition. As demonstrated by AFM and XRD, the use of the MMEE method has shown a better surface morphology of the grown samples and it is more sufficient for strain compensation compared to the MEE method. Also, the devices grown by the MMEE method showed enhanced quantum

efficiency, responsivity and detectivity performance. The dark current density was also reduced by almost one order of magnitude compared to the ones grown by a conventional migration enhanced epitaxy (CME) method. In contrast, Sb segregation is the main obstacle in the growth of Ga-free InAs/InAsSb T2SL. A few studies have indicated the main challenges associated with the growth of Ga-free T2SL through the influence of surface interfaces and Sb segregation on the structural, optical, and electrical properties.^[54,55] This Sb segregation potentially stimulates undesirable effects on bandgap energy shifts including broadening of the PL profile as well as weakened absorption^[114,115] which could lead to degrade the device performance. Recently, Jiang et al.^[116] have grown a MWIR InAs/AlAs/InAsSb T2SL in which the AlAs layers were inserted within the InAs layers for the growth of high-quality strain balanced superlattice.

The performance of T2SL can be improved with the development of advanced, single crystal growth techniques including, MBE and MOCVD and various chemical passivation processes which can enhance device performance. MBE is the preferable growth technique for T2SL materials due to its significantly low growth rate ($\approx 1 \mu\text{m h}^{-1}$) which is useful for controlling both SL layer thicknesses and compositions. In addition, it benefits from low growth temperature, ultrahigh vacuum environment, in situ characterizations for monitoring crystal-quality, and capability for controlled doping and interfacial profiles. In comparison with MBE, MOCVD could enable low-cost and high-yield production of Sbs-based SL since the MOCVD is the leading III–V growth tool in industry. However, due to fundamental properties such as low melting points and low equilibrium vapor pressure, the growth of high-quality Sb-based materials by MOCVD is more challenging.^[38,117] The MOCVD growth of Ga-free InAs/InAsSb T2SL is highly challenging due to the difference in optimal growth conditions for InAs and InAsSb layers. Usually, large arsine (AsH_3) gas flow is preferred for high V/III ratio growth of InAs layers. However, this is not the case for As-rich InAsSb layer growth because the Sb incorporation efficiency is greatly suppressed by the As component which is preferentially incorporated while excess Sb is rejected and left to float on the surface of the epitaxial layer. As a result, a low V/III flux ratio and high trimethylantimony (TMSb)/($\text{TMSb} + \text{AsH}_3$) mole fraction is necessary to achieve high Sb composition during InAsSb layer growth.^[117] Razeghi et al.^[118] used diluted AsH_3 for the MOCVD growth of the InAsSb layer and pure AsH_3 for the InAs layer at a low V/III ratio to enhance Sb incorporation. Although significant work and progress have been made in the growth of InAs/GaSb and InAs/InAsSb T2SL materials and devices by MBE^[102,116,119–123] and MOCVD,^[107,124–130] growth of barrier structures is generally challenging because barrier structures usually contain Al-material such as AlSb, AlAs, or AlAsSb, and Al-containing materials are challenging to grow and susceptible to oxidation during both growth and processing stages. The absence of Al-based barriers could also be associated with the fact that although the lattice mismatches, within the 6.1°A° family of InAs, GaSb, and AlSb are small, they are not negligible particularly at high growth temperatures. Moreover, it has been shown that the MOCVD growth of short periods InAs/GaSb and InAs/InAsSb T2SL structures is further limited by the possibility of decomposition and degradation of the interface quality during growth.^[131–135] Consequently,

Huang et al.^[136–139] have alternatively demonstrated the first MOCVD growth of Al-free InAs/GaSb T2SL PnN barrier structure, which was comprised of a *p-type* mid-wavelength superlattice (MWSL) contact layer (*P*-region) and an *n-type* MWSL barrier layer (*N*-region) and an *n-type* long-wavelength superlattice (LWSL) absorber layer (*n*-region), which resulted in high-quality material growth and high-performance T2SL detectors. For more details about the difficulties associated with the MOCVD growth of Sb-based and other III–V semiconductors, the reader is directed to the review work published by Biefeld.^[117]

2.4. Absorption Coefficient

It is well known that the incident photons are absorbed when $E \geq E_g$, whereas the photons are transmitted when $E < E_g$. If we consider an incident photon with intensity (I) passes through a semiconductor material at some depth (x), then the intensity of photons changes depending on the change in the distance which can be expressed as follows^[140]

$$-\frac{dI(x)}{dx} = \alpha I(x) \quad (3)$$

$$I(x) = I_0 \exp^{-(\alpha x)} \quad (4)$$

where α corresponds to the absorption coefficient which has a unit of cm^{-1} . This coefficient depends mainly on the wavelength of incident photons and material property. It is evident from Equation (4) that the intensity of the photon decreases exponentially with increasing the depth of the material.

Figure 7 shows the absorption coefficient (α) of Ga-free and Ga-based T2SL in the MWIR as a function of wavelength at 77 K. Theoretical and experimental investigations by Klipstein in 2014^[48] revealed that Ga-free T2SL exhibits a slightly weaker optical absorption coefficient ($< 0.2 \mu\text{m}^{-1}$) compared to Ga-based T2SL ($> 0.2 \mu\text{m}^{-1}$) near the cut-off wavelength of the photodetector. This is attributed to the band offsets profile and e–h carrier spatial separation in Ga-free being responsible for reducing the absorption coefficient and lowering the QE performance.

The absorption coefficient of T2SL is determined by the layer thickness, the number of periods and the Sb content of Ga-free InAs/InAsSb SL. A study by Katayama et al.^[141] have shown the effect of increasing the absorption layer on the QE performance. In the study, three structures of Ga-based T2SL *pin* detectors with different absorber thicknesses (1.5, 3, 5, and 10 μm) are theoretically compared. It was found that the 10- μm absorber layer has achieved the highest QE of $\approx 65\%$ at around 4.5 μm , whereas the lowest QE of $\approx 28\%$ is observed with a thinner 1.5 μm absorber layer. Another study by Livneh in 2012^[56] demonstrated that there is perfect agreement between theoretical and experimental values of the absorption coefficient for the Ga-based SL with different layer thicknesses in the MWIR regime at 77 K. To investigate the impact of layer thickness on absorption coefficient, various MWIR Ga-based SL with different GaSb width (10.6 and 15.6 MLs) and fixed InAs width (8.6 MLs) were studied. It was found that when the width of the GaSb layer is increased by ≈ 3 ML, the absorption spectra are shifted to a longer wavelength of $\approx 0.3 \mu\text{m}$. Letka et al.^[142] studied the effect of increasing the periods in the MWIR Ga-free InAs/InAs_{0.82}Sb_{0.18} SL on the

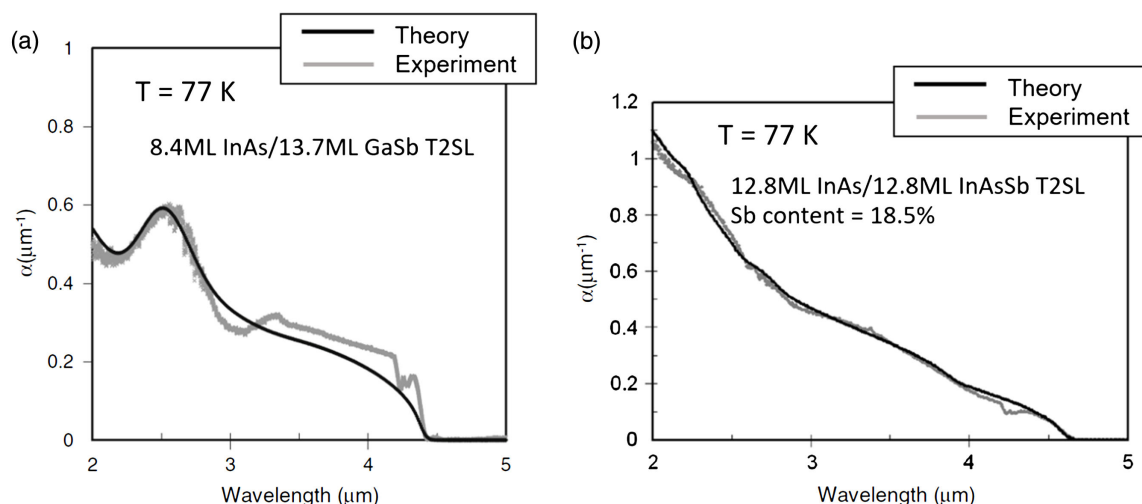


Figure 7. Experimental (grey) and theoretical (black) results of the absorption coefficients as a function of wavelength at 77 K for a) Ga-based InAs/GaSb and b) Ga-free InAs/InAsSb T2SL. Reproduced with permission.^[48] Copyright 2014, Springer Nature.

absorption coefficients while maintaining the same absorber thickness (0.7 μm). It was found that the absorption coefficients are slightly higher for SL with longer periods compared to shorter periods, specifically near the cutoff wavelengths of the detectors. However, they have comparable absorption coefficients in the short wavelength range $\approx 1.5\text{--}3\ \mu\text{m}$. Another study^[143] has attempted to investigate the influence of varying the Sb compositions in the Ga-free SL from 20% to 40%. It was observed that the absorption coefficients increase considerably with increasing the Sb compositions from 20% to 25% which are sensitive to the change in the Sb compositions, particularly in the MWIR region $3\text{--}5\ \mu\text{m}$. However, it seems that at higher Sb compositions (above 20%), the absorption coefficient is roughly insensitive to the Sb concentration. This change in the absorption coefficients is possibly due to the change in the conduction and valence band edges while varying the Sb alloy composition in the Ga-free SL material.

3. Optical and Electrical Performance of PDs

In this section, the performance of Ga-free and Ga-based T2SL PDs are compared including quantum efficiency (QE), detectivity (D^*), signal-to-noise ratio (SNR), dark current density (J), and differential resistance-area product (R_{dA}).

3.1. Quantum Efficiency

Quantum efficiency (QE) is an important characteristic that is generally defined as the conversion of incident photons (input light) into output power. The QE can be evaluated from the photo response measurement using the following equation

$$QE = \frac{1.24 R_i}{\lambda} \quad (5)$$

where R_i is the photodetector's responsivity and λ is the cut-off wavelength. There are two primary terms related to QE which

need to be distinguished. These are internal quantum efficiency (IQE) and external quantum efficiency (EQE). IQE is the fraction of incident photons that enter the detector which is converted into output power at a given energy or wavelength, while EQE is the fraction of incident photons on the detector that is converted into output power at a given energy or wavelength. It can be noticed from Equation (5) that QE is inversely proportional to the cut-off wavelength of the detector, however, the main technological challenge with the fabrication of T2SL detectors is the difficulty of growing a high-quality thick absorber layer that can enhance QE. A recent study^[141] has demonstrated that the EQE of a conventional *pin*, MWIR InAs/GaSb T2SL photodetector, with a cut-off wavelength of $6\ \mu\text{m}$, could be increased from $\approx 25\%$ to $\approx 70\%$ at $4.5\ \mu\text{m}$ by increasing the width of the absorption layer of the T2SL detector from 1.5 to $10\ \mu\text{m}$. It was also suggested that the QE can be further enhanced by employing an anti-reflection coating for the T2SL detectors. The QE of a conventional photodiode is mainly related to the carrier diffusion length.^[14] Hence, the diffusion length factor should be taken into consideration when increasing the width of the absorption layer as increasing the thickness of the absorber layer beyond the minority carrier diffusion length may reduce the QE of the device. This is because photogenerated carriers cannot be collected when the absorption layer thickness exceeds the carrier diffusion length of the photodiode. This challenge can be overcome with the use of a quantum cascade infrared photodetector (QCIPD) design which will be discussed in Section 4.2.

The QE as a function of the absorber thickness of various T2SL photodetector structures are compared at 150 K in **Figure 8**. Data in the plot were accumulated from literature for both barrier and nonbarrier Ga-free^[130,144–148] and Ga-based^[87,149–152] T2SL detectors with different absorber thicknesses, periods, doping concentrations, and bias operations. These factors can significantly affect the performance of the PDs. It is noticeably seen from Figure 8 that the QE of the T2SL PDs is mainly dependent on the absorber thickness. This means that by increasing the T2SL absorber thickness,

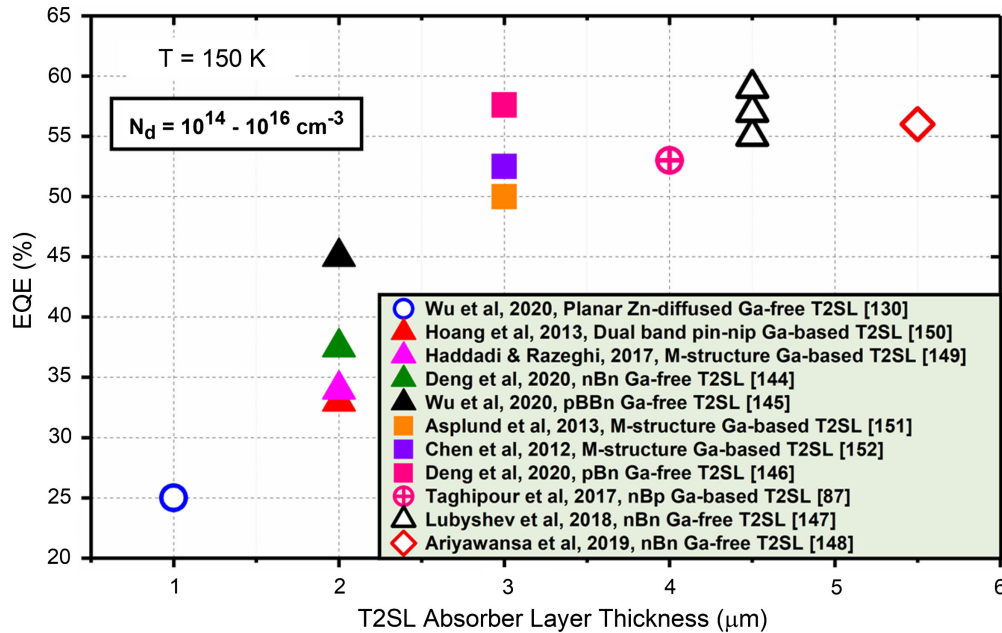


Figure 8. Quantum efficiency versus absorber thickness for Ga-free and Ga-based T2SL barrier and nonbarrier PDs at high temperature of 150 K.

the QE of the detectors is enhanced but taking into consideration the diffusion length factor as demonstrated earlier. It is also evident that the QE for both Ga-free and Ga-based T2SL detectors is roughly ranging from 25% to 60% which is dependent on the T2SL design and absorber thickness.

It is also to be noted that the QE of T2SL is temperature dependent, however, the literature includes somehow contradictory arguments regarding temperature dependence of the minority carrier diffusion length. It has been assumed that the diffusion length decreases at higher temperatures^[153] which is possibly attributed to the decrease in minority carrier lifetime suggested by the known $T^{-1/2}$ dependence of SRH lifetimes. Other reports indicate that the diffusion length is proportional to the temperature. Klipstein et al.^[154] pointed out that the lateral diffusion length varies linearly from 6.3 to 11 μm over the temperature range 78–130 K. This is also consistent with the temperature dependence of diffusion coefficient (D) as expressed by

$$D = \frac{K_B T}{e} \mu \quad (6)$$

where K_B is the Boltzmann constant, T is the temperature, and μ is the mobility. It is to be taken into account that Equation (6) can be only used to measure the lateral diffusion length but not the vertical diffusion length which mainly affects the detector performance. Recently, Taghipour et al.^[85] have attempted to measure the vertical diffusion length of InAs/GaSb T2SL over the temperature range 80–170 K utilizing the electron-beam induced current technique. It has been found that the diffusion length is almost constant at ≈ 1.5 μm over the temperature range 80–140 K and increases to 4.5 μm at 170 K. These results suggest that the QE of the T2SL can be further improved with taking care of the T2SL design and diffusion length factor.

It is also important to note that background doping concentration (intrinsic carrier concentration – n_i) has an effect on the

minority carrier lifetime and hence the QE performance of T2SL detectors. It is found that increasing the doping concentration in the T2SL absorber layer results in a decrease in the QE of the PDs which is possibly due to a decreased minority diffusion length of the minority carriers.^[138] This is suggested by that the intrinsic carrier concentration scales inversely with the MC lifetime ($n_i \sim \tau^{-1}$).^[44] For a more detailed study about the effect of carrier doping concentration on minority carrier lifetime, the reader is directed to the following reports.^[155–158]

3.2. Detectivity

Detectivity (D^*) is inversely proportional to the noise equivalent power (NEP) of the photodetector. NEP is defined as the ratio of the output signal to the input power. However, because the detectivity of the photodetector is influenced by the bandwidth (Δf) and device area (A) measurements, a new term called a specific detectivity was introduced by Jones^[159] which normalizes its detectivity to the device area and bandwidth using the following expression

$$D^* = \frac{\sqrt{\Delta f} \cdot A}{NEP} \quad (7)$$

The specific detectivity can be then determined from the spectral response measurement of the photodetector using the following equation

$$D^* = \frac{R_i}{\sqrt{\frac{4K_B T}{RA} + 2qJ}} \quad (8)$$

where R_i is the spectral responsivity, RA is the dynamic resistance-area product, q is the charge of electron, and J is the dark current density. Here, an analysis of the spectral

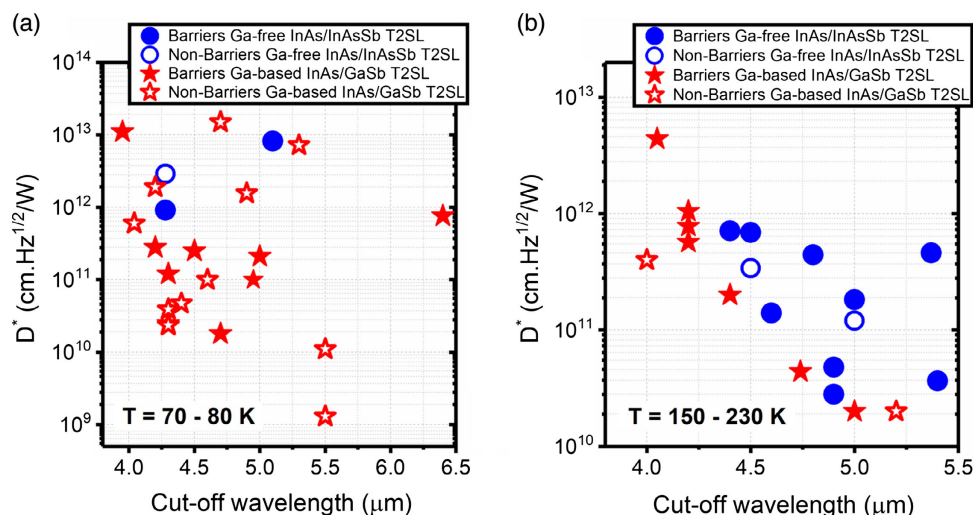


Figure 9. Collected data of detectivity versus cut-off wavelength at a) a low-temperature range from 70 to 80 K and b) a high-temperature range from 150 to 230 K for barrier Ga-free,^[57,129,144–146,160–166] nonbarrier Ga-free,^[118,130,167] barrier Ga-based,^[149,168–176] and nonbarrier Ga-based^[108,173,177–182] T2SL PDs.

detectivity (D^*) of Ga-free and Ga-based T2SL PDs at low and high temperatures in the MWIR regime is presented in **Figure 9**. Interestingly, T2SL PDs with barrier designs have slightly higher detectivities compared to nonbarrier structures particularly at the HOT range, typically in the range of $\approx 3 \times 10^{10}$ to 8×10^{11} cm Hz^{1/2} W⁻¹ (see **Figure 9b**). At a low-temperature range (**Figure 9a**), the D^* of nonbarrier detectors varies from $\approx 10^9$ to 10^{12} cm Hz^{1/2} W⁻¹. A summary of the D^* values of barriers/nonbarriers T2SL, extracted from **Figure 9**, at different applied reverse bias from 30 to 300 mV at low and high operating temperatures is presented in **Table 2**.

3.3. Signal-to-Noise Ratio

Signal-to-noise ratio (SNR or S/N) is another important characteristic that is considered as a figure of merit to evaluate the performance of PDs. SNR is defined as the ratio between the input power of a signal to the output power of background noise and this can be simply expressed as follows

$$SNR = \left(\frac{P_{\text{signal}}}{P_{\text{noise}}} \right) \quad (9)$$

where P_{signal} and P_{noise} are the input power of signal and output power of background noise, respectively. It is always desirable to

Table 2. Typical D^* values of barrier and nonbarrier T2SL PDs at low and high operating temperatures under an applied bias from 30 to 300 mV.

Photodetector design	Material system	D^* at LOT [cm Hz ^{1/2} W ⁻¹]	D^* at HOT [cm Hz ^{1/2} W ⁻¹]
Barrier	Ga-free T2SL	$\approx 9 \times 10^{11}$ – 8×10^{12}	$\approx 3 \times 10^{10}$ – 7×10^{11}
	Ga-based T2SL	$\approx 2 \times 10^{10}$ – 8×10^{11}	$\approx 4 \times 10^{10}$ – 8×10^{11}
Nonbarrier	Ga-free T2SL	$\approx 3 \times 10^{12}$	≈ 1 – 3×10^{11}
	Ga-based T2SL	$\approx 1 \times 10^9$ – 2×10^{12}	$\approx 2 \times 10^{10}$

reduce the background noise including noise voltage, noise current, and shot noise values so that SNR performance can be enhanced. Several studies have been conducted to investigate the SNR ratio of single-pixel PDs based on Ga-free and Ga-based T2SL. A recent study by Kim et al.^[164] examined the performance of Ga-free InAs/InAsSb T2SL photodetector with a barrier structure, achieved a room temperature cut-off wavelength of 5.5 μ m. The noise spectrum for two large and small single-pixels, 1000 and 250 μ m detectors were measured under an applied bias of 200 \times 300 mV with a frequency of 10⁴ Hz. The measured noise voltage was as low as 2.8×10^{-8} V Hz^{-1/2} for the 250 μ m and 1.8×10^{-8} V Hz^{-1/2} for the 1000 μ m detectors. The noise current measurements were also performed on an *nBn* barrier design-based Ga-containing InAs/GaSb T2SL with a diameter of 300 μ m which exhibited a value of around 1×10^{-10} A cm⁻¹ Hz^{1/2} under an applied bias of 300 mV and at room temperature.^[183]

3.4. Dark Current Density

Although the T2SL band structure could be used to suppress Auger nonradiative recombination mechanism,^[28,69] it is crucial to further limit the dark current in a photodetector to enable HOT operation. The dark current is defined as the flow of current through a detector in the absence of light. This leads to the creation of a false signal when there is no photon present in the detector. Therefore, measurement of current–voltage (*I*–*V*) characteristics is an important technique to identify the dominant dark current mechanism within the device. In a photodiode, the dark current could either flow through the bulk or along the surface sidewall of the detector. The dark current density can be expressed as

$$J = \frac{I}{A} = \frac{(I_B + I_S)}{A} = J_B + J_S \left(\frac{P}{A} \right) \quad (10)$$

where I_B and I_S are the bulk and surface dark current, J_B and J_S are the bulk and surface dark current density, and P/A is the ratio of mesa perimeter to the area of the photodiode. In the photodiode, diffusion, generation recombination (G-R) associated with SRH centers, and BTB tunneling currents contribute to the bulk dark current which is independent of the P/A ratio. Conversely, as can be seen from Equation (10), the surface leakage current is strongly dependent on the P/A ratio. Interestingly, surface leakage current can be effectively minimized through the use of various passivation processes.^[184–189] Since the MC lifetime impacts the diffusion current (I_{diff}) of T2SL detectors based on $I_{diff} \sim \tau^{-1}$, diffusion-limited Ga-free T2SL detectors is supposed to significantly perform better than its counterpart Ga-based T2SL detectors because of the longer MC lifetime. However, this has not yet been realized.

The performance of conventional *pin* PDs (nonbarrier structures) at HOT is poor due to the presence of a high dark current with a significant contribution from G-R SRH current. However, in the last decade, various barrier structures have been introduced to photodetector designs to suppress or even eliminate G-R SRH current to enable HOT applications with a significant reduction in dark current and corresponding enhancement in QE and responsivity demonstrated. The development of barrier detectors was initially proposed by Maimon and Wicks in 2006^[190] using *nBn* InAs and InAsSb bulk structures which represents a significant advancement in III–V semiconductors capability. Since then, various T2SL barrier designs have been extensively developed including *nBn*,^[129,148,168,172,183,191,192] *pBn*,^[146,162] *nBp*,^[87,171,193] *pMp*,^[154,194] *niBin*,^[195] *niBn*,^[164,165] *pBiBn*,^[169,170] and complementary barrier infrared detector (CBIRD).^[166,196] Other novel barrier structures include M-structure^[176,197,198] (implemented to suppress the tunneling current which leads to an increase in the doping concentration of the active region, and suppression of diffusion current), W-structure^[199] (incorporated to suppress tunneling and G-R currents), and N-structure^[200–202] (employed to improve the wavefunction overlap of spatially separated electrons and holes leading to enhancement in QE). The fundamental principle behind the incorporation of these barrier layers is the confinement of the electric field zone to the wide bandgap barrier material instead of the absorber region so that the SRH process occurs in the barrier and not in the absorber region.^[192] In addition, the barrier blocks majority carriers (electrons) from the absorber layer while permitting the transport of minority carriers (holes). Moreover, employing barrier architectures facilitates easy implementation of the passivation processes to minimize surface leakage current.^[14] This has resulted in significant improvements in the overall T2SL photodetector's performance with the demonstration of HOT of 150 K^[162] and beyond 190 K^[203,204] in the MWIR region. This could potentially eliminate the need for cryogenic cooling leading to reduced cost, increased portability, and reduction in size, weight, and power consumption (SWaP) of PDs making them suitable for use in IR space applications.^[205] The advancement of T2SL PDs has not only successfully suppressed the dark current density resulting in high performance at HOT but also allowed for the development of CBIRDs^[57,166,206,207] and multicolor (multiband) bias selectable devices.^[150,160,208–210] A CBIRD is a T2SL structure demonstrated by Gunapala's group that utilizes a pair of electron

and hole blocking SL unipolar barriers to mitigate the G-R and surface leakage currents and to achieve high performance devices and enable for the fabrication of HOT FPA detectors. The multicolor bias selectable devices are multispectral band infrared PDs which can cover separate atmospheric windows, including MWIR, LWIR, and VLWIR. The advantages of such devices are that they can offer better discrimination owing to the higher signal contrast observed between wavebands. In addition, the use of multicolor-band devices enables for operating in a wide range of detection with a selective design from MWIR to VLWIR regions. For example, the bias selectable dual-band devices are normally comprised of two T2SL absorber regions or channels and a thin barrier layer inserted in between the two channels. The major benefit of using a dual-band structure is that the two absorption regions can be addressed alternatively by switching the applied bias voltage. Haddadi and Razeghi^[149] have recently reported three-color multiband detectors based on InAs/GaSb/AlSb T2SL used to address the short, extended-short, and mid-wavelength regions with high-performance multispectral band detectors demonstrated. See the recent review work published by Razeghi et al.^[211] for more detail on multicolor bias selectable devices.

Figure 10 shows various designs of barrier structures used to improve photodetector performance. The details of barrier designs and their principles of operation have been reviewed by Martyniuk et al.^[29,212] As shown in Figure 10a,b the barrier layers are sandwiched between two layers having the same or different doping type. Figure 10c shows the M-structure proposed by Razeghi et al.^[198] in 2007. A thin AlSb barrier layer is inserted in the middle of the GaSb layer within the InAs/GaSb T2SL region to block electrons in the conduction band and create a double quantum well for holes in the valence band. The main objective of utilizing the M-structure is to suppress the tunneling current of the photodetector and attain HOT since the minority carrier concentration is exponentially dependent on temperature and minority carrier lifetime decreases with temperature due to Auger recombination process.^[213] The electrical performances of these devices were improved by more than an order of magnitude compared to a nonbarrier structure in which dark current density, differential resistance-area product (R_0A) and spectral detectivity of the detectors exhibited values of around $3.8 \times 10^{-6} \text{ A cm}^{-2}$, $5 \times 10^3 \Omega \text{ cm}^2$ and $1 \times 10^{12} \text{ cm Hz}^{1/2} \text{ W}^{-1}$ at 150 K, respectively, in the MWIR regime.^[176,213] This significant improvement in the performance of single-pixel T2SL PDs has stimulated research interest in FPA PDs (to be discussed in Section 4.1).

Even though significant progress has been made in the growth, fabrication, and band structure engineering of MWIR T2SL for barrier and nonbarrier structures, their performance has not yet reached the performance level of the current state-of-art MCT technology. This is evident in Figure 11 which shows the dark current density as a function of photodetector's cut-off wavelength in comparison with "Rule 07"^[6] at different temperatures for barriers and nonbarriers Ga-free and Ga-based T2SL. Collected data of dark current density from literature with references are shown underneath Figure 11. "Rule 07" is an empirical expression established in 2007 and updated in 2010^[6] which depicts the best accumulated diffusion-limited dark current densities of planar *p-n* MCT MWIR detectors operating at a

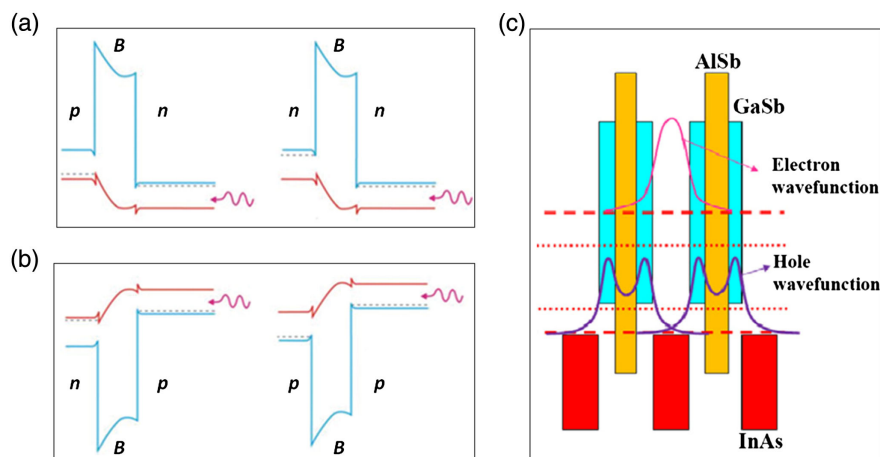


Figure 10. Shows various designs of a) XBn, b) XBP, and c) M-barrier structures. X refers to the contact layers which can be either p-type or n-type as shown on the left-hand side of each structure, B denotes the insertion of barrier into the structure and the active region is on the right-hand side of each structure. The M-structure inserts an AlSb barrier layer between the GaSb layers in the SL region of InAs/GaSb. a,b) Reproduced with permission.^[214] Copyright 2015, Elsevier. c) Reproduced with permission.^[213] Copyright 2020, Elsevier.

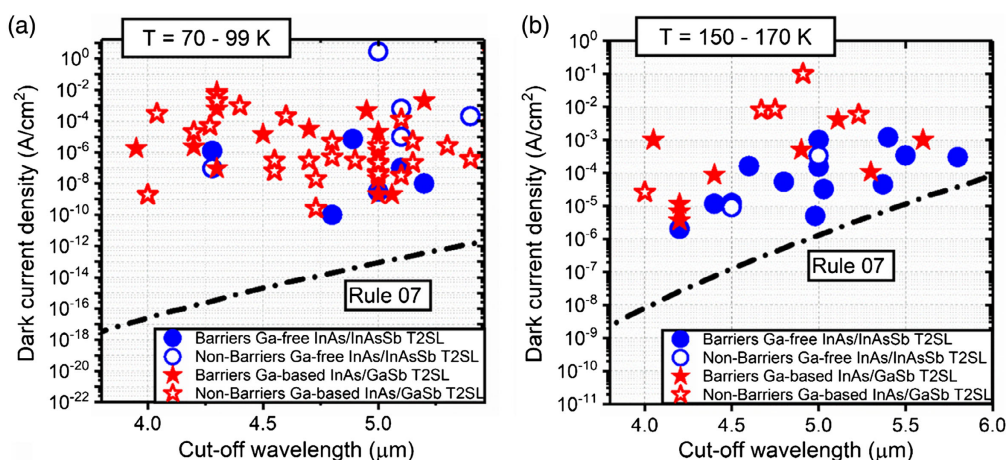


Figure 11. Collected data of dark current density versus cut-off wavelength in the MWIR regime at two different temperature ranges a) from 70 to 99 K and b) from 150 to 170 K for barrier Ga-free,^[22,57,82,83,129,144–148,160–163,166,192,223,224] nonbarrier Ga-free,^[118,130,167,220–222,225] barrier Ga-based,^[87,149,168,170,172,174–176,183,193,219,226–228] and nonbarrier Ga-based^[68,101,108,111,173,177–179,181,189,215–218,229–237] T2SL PDs in comparison with “Rule 07.”

temperature above 77 K and fabricated at Teledyne Imaging Sensors. Figure 11a shows the photodetector’s dark current density at low temperatures between 70 and 99 K. It can be seen that Ga-free (barriers and nonbarriers based) T2SL studies are limited compared to their Ga-based counterparts. The dark current density of the nonbarrier Ga-based T2SL PDs is roughly in the range of 10^{-5} – 10^{-7} A cm⁻² (with some higher outliers) under an applied bias of 50–200 mV for intermediate temperatures of 70–99 K in the MWIR range.^[101,111,181,215–218] The best performing T2SL photodetector was reported by Schmidt et al.^[219] in 2017 using a P⁺ N⁻ Ga-based T2SL barrier structure with a cut-off wavelength of ≈ 4.7 μ m achieved at 77 K. A very low dark current density ($J \sim 2.6 \times 10^{-10}$ A cm⁻²) was achieved under an applied bias of 100 mV. In contrast, nonbarriers, Ga-free T2SL exhibit a slightly higher dark current density compared to Ga-

based T2SL with dark current density is in the range of 10^{-3} – 10^{-5} A cm⁻² (with some higher/lower outliers) at an applied bias of 10–300 mV at the same operating temperatures.^[220–222] Recently, a very low dark current density of around 9.6×10^{-8} A cm⁻² has been reported at an applied bias of 20 mV and 77 K using a nonbarrier, Ga-free T2SL, for a Zn-diffused planar photodetector grown by MOCVD.^[130] It can be seen from Figure 11a that the lowest dark current density so far of $J \sim 1 \times 10^{-10}$ A cm⁻² has been achieved at an applied bias of 100 mV and 99 K using a Ga-free T2SL, *nBn* design.^[83] Generally, the best performing T2SL PDs with low dark current densities are achieved using barrier structures that are roughly four to five orders of magnitude higher than “Rule 07” at low operating temperatures (70–99 K) in the MWIR range. The variation in dark current density performance, due to changes in

T2SL designs and growth on nonnative substrates, highlights the importance of utilizing barrier structures to minimize the contribution of G-R dark current and to assist for surface passivation which can also be implemented to reduce the contribution of surface leakage current. However, band offsets engineering of the barrier detector is a crucial aspect that needs to be considered in designing such a structure. The zero band offsets alignments are critically important for enhanced device performance without impeding the flow of carriers. Another aspect is the fabrication and etching process of Al material-based barrier detectors which could have an effect on the absorber region and limit the device performance. This means that by etching the Al-based barrier detectors, Al material is easily oxidized when it is wet etched and can result in the formation of an oxidation layer at the surface of the absorber layer which can hamper the flow of current and limit the device characteristics. Consequently, there is an essential need for Al-free barrier layers with zero band offsets to improve the performance of InAs/GaSb and InAs/InAsSb T2SL materials.

Figure 11b shows the dark current densities of the PDs at high temperatures between 150 and 170 K. It can be seen that there is high research interest in barriers-based Ga-free compared to Ga-based T2SL which indicates the potential of Ga-free T2SL to outperform Ga-based T2SL at HOT due to the suppression of G-R SRH related dark current in addition to its appealing fundamental material properties. The best performing T2SL realized using barrier designs where the dark current densities are only about one to two orders of magnitude higher than “Rule 07.” Particularly, the lowest dark current density reported so far by using an *nBn* barrier Ga-free T2SL design with $J \sim 5 \times 10^{-6} \text{ A cm}^{-2}$, obtained at a cut-off wavelength of $\approx 4.9 \mu\text{m}$ at 150 K and under an applied bias of 100 mV, which is only $5 \times$ the MCT’s “Rule 07.”^[83] These barrier-based T2SL PDs with such low dark current densities are highly promising for HOT and can favorably compete with the dominant MCT detectors.

3.5. Differential Resistance-Area Product

Differential resistance-area product (R_dA) is the well-known figure of merit of a photovoltaic detector and can be expressed as

$$R_dA = \left(\frac{\partial J_{\text{dark}}}{\partial V} \right)^{-1} \quad (11)$$

where R_0 is the resistance at zero-bias and J_{dark} is the dark current density. R_dA product is the dynamic resistance-area product that is used for barrier detectors where an applied bias is required to achieve proper responsivity. **Figure 12** compares the R_dA product to “Rule 07” for barrier and nonbarrier PDs based on Ga-free^[163–165,238] and Ga-containing^[68,112,174,182,239] T2SL at HOT of 300 K in the MWIR spectral range. Generally, it can be seen that the RA performance of T2SL PDs is approaching the performance level of the current state-of-the-art MCT detectors. It is seen that the best RA product is achieved using a barrier-based Ga-free T2SL PD,^[163,238] with a cut-off wavelength of $5.8 \mu\text{m}$ under an applied bias of 200 mV, which slightly exceeds the MCT’s “Rule 07” at 300 K. In contrast, the RA performance of nonbarriers Ga-based T2SL^[68,112,182] is lower than that of barrier

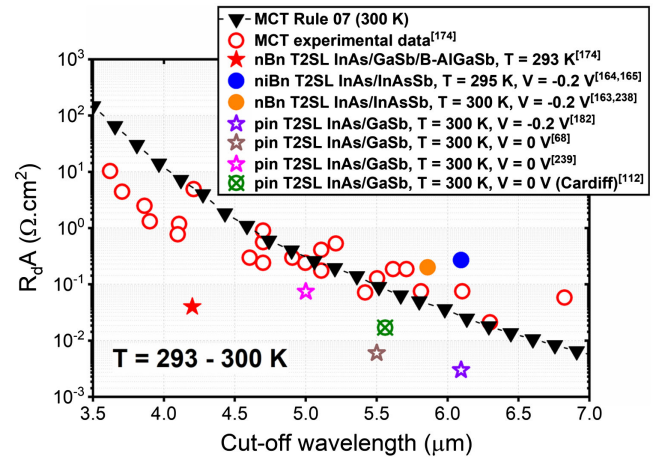


Figure 12. Collected values of R_dA product versus cut-off wavelength for barrier and nonbarrier Ga-free and Ga-based T2SL PDs compared to MCT experimental data and Rule 07 at HOT of 300 K.

detectors and it is roughly less than an order of magnitude compared to “Rule 07.”

4. Recent Advances in IR Detection Technologies

Several advances in IR detection technologies have been developed to realize HOT detection that circumvents the need for cryogenic cooling and satisfy the essential requirement of SWaP. III-V HOT IR detectors are potentially less expensive with high-performance, significantly reduced dark current density, high spectral detectivity and quantum efficiency. In this section, we briefly discuss novel technologies and future approaches of HOT IR photodetection including FPAs and QCIPDs.

4.1. Focal Plane Arrays

A FPA is an array detector that is typically a two-dimensional (2D) array of many pixels. The FPA is commonly used for imaging purposes, but it can also be used for applications in spectrometry and light detection and ranging. Currently, the two main MWIR FPA technologies are either based on InSb or MCT materials, each with its distinct advantage. InSb dominates the MWIR FPA market due to its superior manufacturability and its applicability on PDs systems. In contrast, HgCdTe (MCT) semiconductor can achieve low dark current and higher operating temperature which is, therefore, a detector of choice for more demanding applications. FPA based on T2SL can combine the advantages of III-V semiconductors and the high performance of MCT.

Over the last decade, there has been much progress and developments using the Sb-based IR III-V semiconductors as single-pixel and FPA detectors based on barrier structures which have shown promising results in reducing the G-R dark current enabling HOT with improvement in photodetector’s performance.^[21–23,190,240–243] For the FPA detectors, it is a crucial requirement to not only reduce the cooling power by enabling the noncryogenic operation but also to achieve good operability,

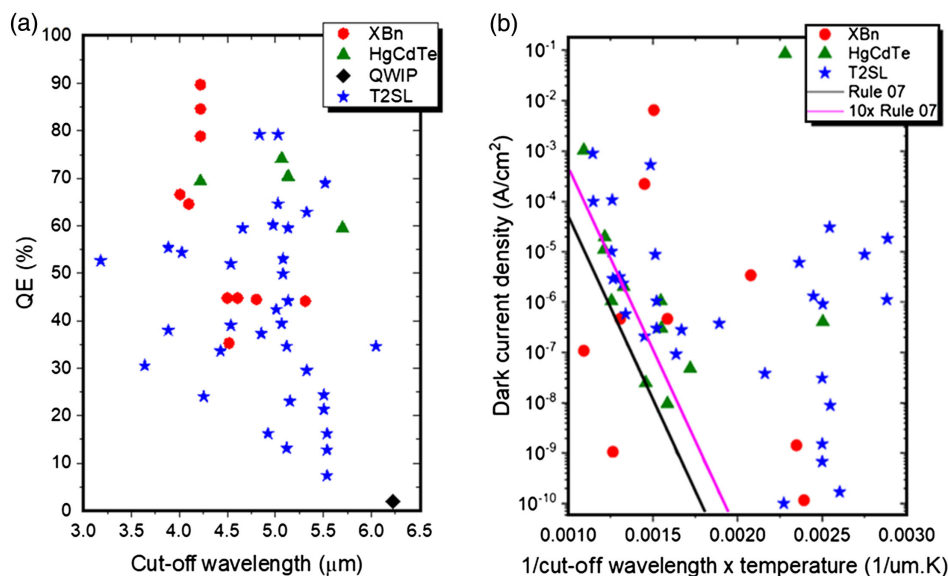


Figure 13. Schematic plots show a) quantum efficiency and b) dark current density performance of current state-of-the-art technologies including XBn, MCT, QWIP, and T2SL single-pixels and FPAs in the MWIR spectral band (3–6 μm). Reproduced with permission.^[250] Copyright 2019, Elsevier.

uniformity, stability, reproducibility, and scalability via fabricating large format and small pitch FPAs. In recent years, developments of Ga-based InAs/Ga(In)Sb and Ga-free InAs/InAsSb T2SL have been carried out by several groups targeted at MWIR^[57,226,244–247] and LWIR^[247–249] FPAs. **Figure 13a** summarizes the quantum efficiency of current state-of-the-art detector technologies including MCT, QWIP, *nBn*, and T2SL FPAs in the MWIR regime. It is clearly shown that the performance of T2SL can compete favorably with these technologies, specifically with the MCT, with the QE of T2SL is in the range of 30–80%.^[250] Although the demonstrated dark current density of SL detectors is reducing and approaching that of MCT detectors, it has still not reached the MCT's "Rule 07" performance level^[6,250] as shown in **Figure 13b**. Theoretically, it is believed that this SL has the potential to considerably exceed the performance of MCT.^[6]

To evaluate the FPAs sensitivity performance, the noise equivalent temperature difference (NETD) characteristic is considered as a primary figure of merit to investigate the reproducibility and stability of the fabricated detectors. As an illustration, the temporal noise is measured via the signal-to-time ratio, whereas the spatial noise is determined by the deviation of pixels in the arrays when illuminated by a uniform and stable black body source. The temporal NETD is defined as the average temporal noise of all pixels in the array with the response per temperature. The spatial NETD is defined as the average spatial noise of deviation values divided by the response per temperature. Hence, a photodetector can achieve good thermal sensitivity when the NETD is minimum. The NETD can be calculated using the formula adduced by Kinch^[5]

$$NETD \propto \frac{\sqrt{J_{\text{dark}} + J_{\text{photon flux}}}}{QE} \quad (12)$$

The NETD is a dark current density-dependent which means that the FPA detector attains lower NETD when the dark current

density is minimal. Recently, IR FPAs based on Ga-containing InAs/GaSb MWIR T2SL barrier structures have been manufactured by the group at IRnova with pixel formats of 320 × 256 and 640 × 512 on 30 and 15 μm pitch, respectively, utilizing a readout integrated circuit (ROIC).^[226,251] The PDs exhibited a cut-off wavelength of 5.1 μm and a low dark current density of $1 \times 10^{-6} \text{ A cm}^{-2}$ with QE of 53% measured under an applied bias of 50 mV at 120 K. The temporal and spatial NETD have been measured for these fabricated FPAs with a demonstration of relatively low NETD values of 12 and 4 mK for the 320 × 256 and 25 and 10 mK for the 640 × 512 with averaged FPAs operability of 99.8% (see **Figure 14a,b**). The 320 × 256 MWIR FPAs detector showed the capability of detecting harmful gases at HOT, such as methane (see **Figure 15a**). Another study by Zhou et al.^[252] in 2016 demonstrated HOT FPAs using 384 × 288 pixels MWIR, Ga-based *pin* T2SL with a small pitch of 25 μm. The fabricated FPA detectors were isolated using a combination of dry and wet etching processes and passivated with SiN_x layer with a fill factor of more than 85% achieved. The detectors with cut-off wavelengths of 4.1 and 5.6 μm exhibited a low dark current density of $5 \times 10^{-10} \text{ A cm}^{-2}$ under an applied bias of 20 mV with NETD of ≈18 mK obtained in the temperature range of (77–100 K) and 10 mK at 77 K. The fabricated FPA exhibited high-quality imaging capability at HOT which demonstrates the good temperature tolerance of the device (see **Figure 15b**).

Ga-free InAs/InAsSb T2SL has been utilized to fabricate FPA detectors. A recent study by Ting et al.^[57] in 2018 reported a HOT MWIR FPA based on *CBIRD* with a cut-off wavelength of 5.4 μm at 150 K. The detector pixels were defined by a dry etch process into a 640 × 512 format on 24 μm pitch using ROIC. The FPA exhibited a low NETD of 18.5 mK and a highly stable-NETD operability of 99.7% in the temperature range of (80–150 K). **Figure 16** shows the images taken with the FPA at 160–170 K in the MWIR range. The Vital Infrared Sensor Technology

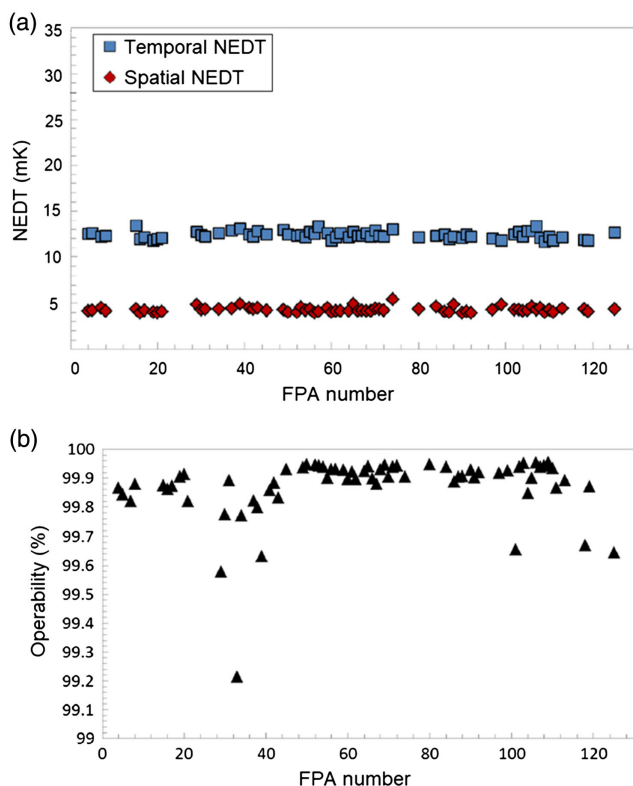


Figure 14. Measurements of a) temporal and spatial NETD of the fabricated FPAs at IRnova showing NETD values and b) operability of FPAs showing a value of around 99.8%. Reproduced with permission.^[226] Copyright 2017, Elsevier.

Acceleration (VISTA), a program developed by the USA government, has recently fabricated large-format dual-band FPA detectors (1280×720) on $12 \mu\text{m}$ pitch which showed excellent manufacturability and high uniformity^[253] (see Figure 17). The NETD value of the FPA was 27.44 mK with operability of 99.09%. These results demonstrate that T2SL detectors with better uniformity over a large area and good performance at a high temperature can favorably compete with the current MCT detectors.

Aim Infrarot-Module GmbH (AIM) has recently manufactured FPAs based p-on-n planar MCT detectors with a cut-off wavelength of $5.2 \mu\text{m}$ achieved at 80 K.^[254] These detectors were fabricated into 640×512 and 1024×768 pixel formats with a 20- and $10\text{-}\mu\text{m}$ pitch, respectively. The NETD performance obtained for the 640×512 FPA detector showed slightly higher values of 24 mK at 160 K with a significant increase to about 40 mK at 180 K. This increase was attributed to the impact of thermal generation dark current which affects the NETD detector's performance and leads to a reduction in integration time. The operability of the FPA detectors was in the range of 99.8–99.5% at 160–170 K. Figure 18 shows the quality of the images taken by the 640×512 pixel on a $20\text{-}\mu\text{m}$ pitch MCT detector array. As shown, for operating temperatures from 120 to 180 K, the quality of images is good, but when temperature was increased above 200 K the dark current contribution became apparent with a considerable increase in noise.

4.2. Quantum Cascade Infrared Photodetectors

Quantum cascade infrared photodetectors (QCIPDs) are multi-stage IR detectors designed to increase quantum efficiency and achieve HOT with low SNR. As discussed previously in Section 3.1, the QE of the photodetector can be enhanced by increasing the thickness of the absorber layer. However, as earlier pointed out, the QE of a conventional photodiode is limited by the carrier diffusion length.^[14] Hence, the diffusion length factor has to be considered when increasing the absorber thickness since increasing the thickness of the absorber layer beyond the carrier diffusion length might not result in the desired parameters enhancement. This means a collection of carriers can only occur when the photogenerated carriers travel a distance less than or equal to the diffusion length of the carriers. In the QCIPDs, each absorber layer is engineered to be ultimately shorter than the diffusion length to enable the collection of all photogenerated carriers. QCIPDs are classified into two groups: 1) Inter-band quantum cascade infrared photodetectors (IB-QCIPDs) and 2) inter-subband quantum cascade infrared photodetectors (IS-QCIPDs). Figure 19 is a schematic diagram of the IB-QCIPDs with absorbers based on Ga-containing InAs/Ga(In)Sb. As shown, there are different zones, and each zone has its mechanism: 1) The excitation zone (absorbing layer)



Figure 15. a) An image captured by IRnova camera with the fabricated 320×256 MWIR FPA on a $30\text{-}\mu\text{m}$ pitch showing detection of methane gas. It can be seen that the methane cloud (seen as a black cloud in the image) is observed around the nozzle. Reproduced with permission.^[251] Copyright 2016, SPIE. b) An image was taken by the fabricated 384×288 MWIR FPA on a $25\text{-}\mu\text{m}$ pitch. Reproduced with permission.^[252] Copyright 2016, Elsevier.

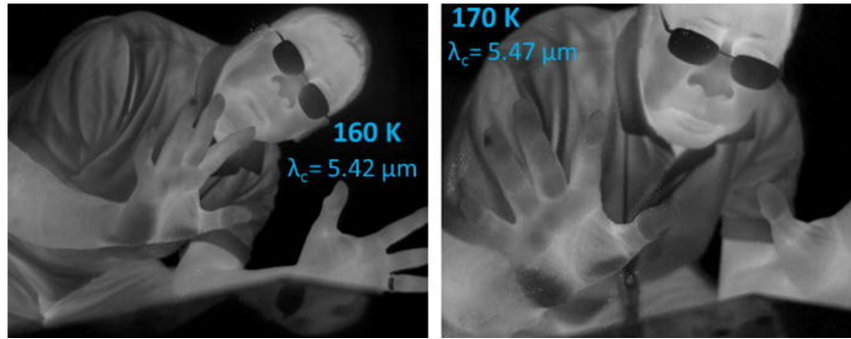


Figure 16. Images captured by the fabricated Ga-free T2SL 640×512 MWIR FPA on a $24\text{-}\mu\text{m}$ pitch. It can be seen that good-quality images are obtained in the MWIR domain at HOT of 160–170 K. Reproduced with permission.^[166] Copyright 2018, AIP Publishing.



Figure 17. An image captured with 1280×720 dual-band FPA detector on a $12\text{-}\mu\text{m}$ pitch based on Ga-free T2SL. The image was taken at 80 K with $f/4$ optics. Reproduced with permission.^[253] Copyright 2017, SPIE.

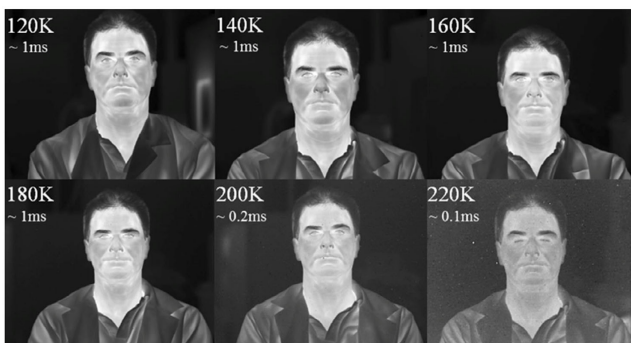


Figure 18. Images captured by MWIR MCT FPA 640×512 with a $20\text{-}\mu\text{m}$ pitch at operating temperatures from 120 to 220 K. Reproduced with permission.^[254] Copyright 2017, Springer Nature.

where electrons are excited from the valence band to the conduction band by the absorption of photons. 2) The intraband relaxation zone has electron and hole barriers consisting of digitally graded AlSb/GaSb multi-quantum wells (MQWs) barrier for electrons and InAs/AlSb MQWs barrier for holes. In this region, electrons are transported, and holes confined to zones (1) and (3). In region (3), the inter-band tunneling zone, electrons return to the valence band of the absorbing layer via the tunneling mechanism.

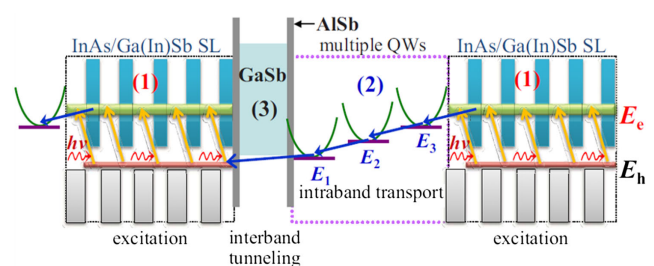


Figure 19. A schematic diagram shows the IB-QCIPDs using Ga-based T2SL absorbers. Reproduced with permission.^[255] Copyright 2010, AIP Publishing.

The main difference between IS-QCIPDs and IB-QCIPDs is that the transition in IS-QCIPDs occurs within the same band (e.g., the conduction band), whereas the transitions occur between the conduction band and the valence band in the IB-QCIPDs. Fundamentally, the IB-QCIPDs and IS-QCIPDs are very different in terms of activated processes and distinct carrier lifetimes, that is, IS-QCIPDs have a fast rate of phonon scattering in the range of picosecond while nanosecond range for Auger and SRH recombination in IB-QCIPDs.^[256] Based on more than two decades of investigations on IS-QCIPDs and IB-QCIPDs, it is well known that the IB-QCIPDs have a relatively much longer minority carrier lifetime which has led to a significantly lower dark current density and higher performance compared to the IS-QCIPDs at room temperature.^[256] IB-QCIPDs T2SL have shown promising results including HOT above 290 K and up to 450 K,^[255,257–259] high spectral detectivity of $>10^9$ Jones at 300 K^[259,260] and QE of 55% at 200 K.^[261] A recent published review work has compared the PDs' performances of IB-QCIPDs based on SL, IS-QCIPDs, and QWIPs in the MWIR and LWIR regions at 300 K.^[256] This comparative study of electrical performances including spectral responsivity and peak detectivity showed that the photodetector performance of the IB-QCIPDs is much higher than that of IS-QCIPDs. Another study^[262] has experimentally demonstrated that the R_0A products of the IB-QCIPDs T2SL are higher than the MCT photodiodes. **Figure 20** compares the R_0A product as a function of cut-off wavelength for IB-QCIPDs based on InAs/GaSb T2SL,^[255,257,259,262–264] IS-QCIPDs based on InGaAs/InAlAs

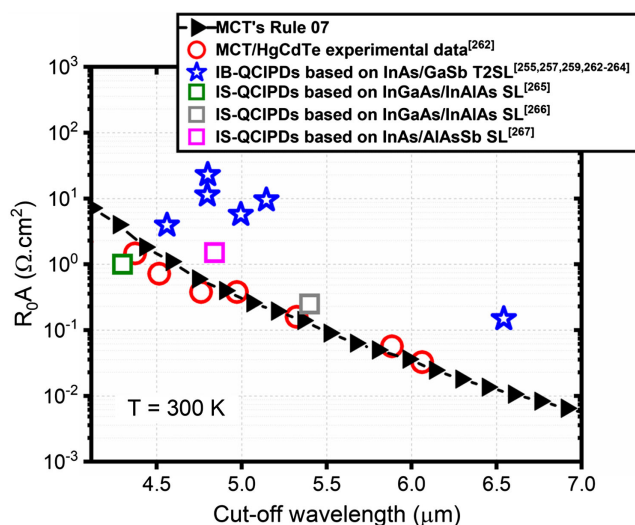


Figure 20. Collected values of R_0A product versus cut-off wavelength of IB-QCIPDs based on InAs/GaSb T2SL, IS-QCIPDs SL based on InGaAs/InAlAs and InAs/AlAsSb in comparison with MCT photodiodes at 300 K.

SL^[265,266] and InAs/AlAsSb SL,^[267] and MCT photodiodes^[262] at 300 K. It can be seen that R_0A for the IB-QCIPDs is higher than that for IS-QCIPDs and it is significantly exceeding the MCT's "Rule 07" at 300 K.

5. Conclusion

In this review, the fundamental optical properties of T2SL material systems have been evaluated including bandgap energies, band heterostructure alignments, absorption coefficients, and minority carrier lifetimes. In addition, materials growth method of Ga-free and Ga-based T2SL has been compared. Moreover, the photodetector's optical and electrical performances for both Ga-free and Ga-based T2SL have been compared with respect to quantum efficiency, detectivity, dark current density, and differential resistance-area product in the MWIR domain. It has been shown that the QE of Ga-free and Ga-based, barriers-based T2SL is typically in the range of 25 to $\approx 60\%$ at high temperature (150 K). This QE performance is comparable to the current state-of-the-art MCT detectors at HOT. It has been also highlighted that the QE of T2SL detectors can be increased by increasing the absorber thickness but not beyond the diffusion length. Furthermore, the dark current densities of nonbarriers based, Ga-containing T2SL are slightly lower (10^{-7} – 10^{-5} A cm^{-2}) than that of Ga-free T2SL (10^{-5} – 10^{-3} A cm^{-2}) at low temperatures (70–99 K). However, barriers-based, Ga-free T2SL have shown slightly lower dark current densities compared to Ga-based T2SL at HOT (150–170 K) with more research focused on Ga-free T2SL in this temperature range. A rule of thumb called "Rule 07" has been used to compare the dark current densities of both T2SL with MCT detectors at low and high operating temperatures. It has been shown that the best performing barriers based T2SL dark current densities are as far as four to five orders of magnitude higher than "Rule 07" at low operating temperatures, whereas they are only about one to two orders of

magnitude closer to "Rule 07" at high operating temperatures in the MWIR spectral range. In addition, the differential resistance-area products of both T2SL at HOT have been compared. It has been shown that RA products of Ga-free T2SL barrier detectors are slightly exceeding "Rule 07." In contrast, the RA products of nonbarrier Ga-based T2SL detectors are only a few times the MCT's "Rule 07" at 300 K.

Due to the interesting material properties of T2SL and the outstanding optical and electrical performances demonstrated, they are emerging as a highly promising material for use in the future generation of IR detectors and as an alternative to the current state-of-the-art MCT. As a result, new designs and approaches are currently being explored including FPAs and novel multi-stage detector architectures such as QCIPDs. T2SL have demonstrated enormous promise with the potential to outperform the current state-of-the-art HOT MCT detectors. They have the potential to operate at HOT and satisfy the SWaP requirement to avoid the need for cryogenic cooling which is the primary limiting factor for the MCT detectors.

Acknowledgements

One of the authors, D.O.A., acknowledges the Saudi Arabia government for the Ph.D. scholarship provided via the University of Bisha (UB), Ministry of Education. The authors hereby acknowledge the following research groups, whom their findings have significantly contributed to improve the detectors research field. These research groups are M. Razeghi (Center for Quantum Devices – Northwestern University), A. Rogalski (Military University of Technology), S.D. Gunapala (Jet Propulsion Lab), and Y.-H. Zhang (Arizona State University).

Conflict of Interest

The authors declare no conflict of interest.

Keywords

barrier detectors, high operating temperature, InAs/GaSb, InAs/InAsSb, mid-wavelength infrared, type-II superlattices

Received: March 28, 2021

Revised: August 30, 2021

Published online:

- [1] D. A. Bui, P. C. Hauser, *Anal. Chim. Acta* **2015**, 853, 46.
- [2] D. Jung, S. Bank, M. L. Lee, D. Wasserman, *J. Opt.* **2017**, 19, 123001.
- [3] L. Fleming, D. Gibson, S. Song, C. Li, S. Reid, *Surf. Coat. Technol.* **2018**, 336, 9.
- [4] M. Villar, Master Thesis, University of Central Florida, **2017**.
- [5] M. A. Kinch, *Fundamentals of Infrared Detector Materials*, SPIE Press, Bellingham, WA **2007**.
- [6] W. E. Tennant, *J. Elec. Mater.* **2010**, 39, 1030.
- [7] P. Knowles, L. Hipwood, L. Pillans, R. Ash, P. Abbott, *Proc. SPIE* **2011**, 8185, 818505.
- [8] L. Rubaldo, A. Brunner, P. Guinedor, R. Taalat, D. Sam-giao, A. Kerlain, L. Dargent, P.-L. Nicolas, V. Chaffraix, M.-L. Bourqui, Y. Loquet, J. Coussement, *Proc. SPIE* **2016**, 9819, 981911.
- [9] W. Gawron, A. Damiński, A. Koźniowski, P. Martyniuk, K. Stasiewicz, P. Madejczyk, J. Rutkowski, *IEEE. Sens. J.* **2020**, 21, 1.

- [10] M. A. Kinch, F. Aqariden, D. Chandra, P.-K. Liao, H. F. Schaake, H. D. Shih, *J. Elec. Mater.* **2005**, *34*, 880.
- [11] S. Krishnamurthy, M. A. Berding, Z. G. Yu, *J. Elec. Mater.* **2006**, *35*, 1369.
- [12] A. Rogalski, *Rep. Prog. Phys.* **2005**, *68*, 2267.
- [13] A. Rogalski, *HgCdTe Photodetectors*, Woodhead Publishing, **2020**, <https://doi.org/10.1016/B978-0-08-102709-7.09993-9>.
- [14] A. Rogalski, P. Martyniuk, M. Kopytko, *Prog. Quantum Electron.* **2019**, *68*, 100228.
- [15] A. Evirgen, J. Abautret, J. P. Perez, H. Ait-Kaci, P. Christol, J. Fleury, H. Sik, A. Nedelcu, R. Cluzel, A. Cordat, *Proc. SPIE* **2014**, 8993, 899313.
- [16] A. Evirgen, J. Abautret, J. P. Perez, A. Cordat, A. Nedelcu, P. Christol, *Electron. Lett.* **2014**, *50*, 1472.
- [17] J.-P. Perez, A. Evirgen, J. Abautret, P. Christol, A. Cordat, A. Nedelcu, *Proc. SPIE* **2015**, 9370, 93700N.
- [18] P. Klipstein, D. Aronov, M. ben Ezra, I. Barkai, E. Berkowicz, M. Brumer, R. Fraenkel, A. Glozman, S. Grossman, E. Jacobsohn, O. Klin, I. Lukomsky, L. Shkedy, I. Shtrichman, N. Snapi, M. Yassen, E. Weiss, *Infrared Phys. Technol.* **2013**, *59*, 172.
- [19] G. Deng, W. Yang, P. Zhao, Y. Zhang, *Appl. Phys. Lett.* **2020**, *116*, 031104.
- [20] G. Deng, W. Yang, X. Gong, Y. Zhang, *Infrared Phys. Technol.* **2020**, *105*, 103260.
- [21] P. Klipstein, O. Klin, S. Grossman, N. Snapi, B. Yaakovovitz, M. Brumer, I. Lukomsky, D. Aronov, M. Yassen, B. Yofis, A. Glozman, T. Fishman, E. Berkowitz, O. Magen, I. Shtrichman, E. Weiss, *Proc. SPIE* **2010**, 7660, 76602Y.
- [22] P. Klipstein, O. Klin, S. Grossman, N. Snapi, I. Lukomsky, D. Aronov, M. Yassen, A. Glozman, T. Fishman, E. Berkowicz, O. Magen, I. Shtrichman, E. Weiss, *Opt. Eng.* **2011**, *50*, 061002.
- [23] P. Klipstein, O. Klin, S. Grossman, N. Snapi, I. Lukomsky, M. Brumer, M. Yassen, D. Aronov, E. Berkowitz, A. Glozman, T. Fishman, O. Magen, I. Shtrichman, E. Weiss, *Proc. SPIE* **2011**, 8012, 80122R.
- [24] A. Soibel, C. J. Hill, S. A. Keo, L. Höglund, R. Rosenberg, R. Kowalczyk, A. Khoshakhlagh, A. Fisher, D. Z.-Y. Ting, S. D. Gunapala, *Appl. Phys. Lett.* **2014**, *105*, 023512.
- [25] A. Rogalski, *Infrared Phys. Technol.* **2011**, *54*, 136.
- [26] H. Wen, E. Bellotti, *Appl. Phys. Lett.* **2015**, *107*, 222103.
- [27] S. R. Kurtz, R. M. Biefeld, A. J. Howard, *Appl. Phys. Lett.* **1995**, *67*, 3331.
- [28] C. M. Ciesla, B. N. Murdin, C. R. Pidgeon, R. A. Stradling, C. C. Phillips, M. Livingstone, I. Galbraith, D. A. Jaroszynski, C. J. G. M. Langerak, P. J. P. Tang, M. J. Pullin, *J. Appl. Phys.* **1996**, *80*, 2994.
- [29] A. Rogalski, P. Martyniuk, *J. Elec. Materi.* **2014**, *43*, 2963.
- [30] G. C. Osbourn, L. R. Dawson, R. M. Biefeld, T. E. Zipperian, I. J. Fritz, B. L. Doyle, *J. Vac. Sci. Technol., A* **1987**, *5*, 3150.
- [31] A. Rogalski, M. Kopytko, P. Martyniuk, *Proc. SPIE* **2017**, 10177, 1017715.
- [32] J. Bajaj, G. Sullivan, D. Lee, E. Aifer, M. Razeghi, *Proc. SPIE* **2007**, 6542, 65420B.
- [33] L. Esaki, R. Tsu, *IBM J. Res. Dev.* **1970**, *14*, 61.
- [34] D. L. Smith, C. Mailhot, *J. Appl. Phys.* **1987**, *62*, 2545.
- [35] G. A. Sai-Halasaz, R. Tsu, L. Esaki, *Appl. Phys. Lett.* **1977**, *30*, 651.
- [36] H. Sakaki, L. L. Chang, G. A. Sai-Halasaz, C. A. Chang, L. Esaki, *Solid State Commun.* **1978**, *26*, 589.
- [37] R. H. Miles, D. H. Chow, Y.-H. Zhang, P. D. Brewer, R. G. Wilson, *Appl. Phys. Lett.* **1995**, *66*, 1921.
- [38] R. M. Biefeld, K. C. Baucom, S. R. Kurtz, *J. Cryst. Growth* **1994**, *137*, 231.
- [39] M. J. Pullin, P. J. P. Tang, S. J. Chung, C. C. Phillips, R. A. Stradling, *Inst. Phys. Conf. New Mexico* **1995**, *144*, 8.
- [40] Y. Zhang, *Appl. Phys. Lett.* **1995**, *66*, 118.
- [41] M. Razeghi, B.-M. Nguyen, *Rep. Prog. Phys.* **2014**, *77*, 082401.
- [42] E. H. Steenbergen, G. Ariyawansa, C. J. Reyner, G. D. Jenkins, C. P. Morath, J. M. Duran, J. E. Scheihing, V. M. Cowan, *Proc. SPIE* **2017**, 10111, 1011104.
- [43] A. Rogalski, P. Martyniuk, M. Kopytko, P. Madejczyk, S. Krishna, *Sensors* **2020**, *20*, 7047.
- [44] L. Höglund, D. Z. Ting, A. Khoshakhlagh, A. Soibel, C. J. Hill, A. Fisher, S. Keo, S. D. Gunapala, *Appl. Phys. Lett.* **2013**, *103*, 221908.
- [45] B. V. Olson, E. A. Shaner, J. K. Kim, J. F. Klem, S. D. Hawkins, L. M. Murray, J. P. Prineas, M. E. Flatté, T. F. Boggess, *Appl. Phys. Lett.* **2012**, *101*, 092109.
- [46] D. Z. Ting, A. Khoshakhlagh, A. Soibel, C. J. Hill, S. D. Gunapala, *Proc. SPIE* **2012**, 8511, 851104.
- [47] A. D. Prins, M. K. Lewis, Z. L. Bushell, S. J. Sweeney, S. Liu, Y.-H. Zhang, *Appl. Phys. Lett.* **2015**, *106*, 171111.
- [48] P. C. Klipstein, Y. Livneh, A. Glozman, S. Grossman, O. Klin, N. Snapi, E. Weiss, *J. Elec. Materi.* **2014**, *43*, 2984.
- [49] I. Vurgaftman, G. Belenky, Y. Lin, D. Donetsky, L. Shterengas, G. Kipshidze, W. L. Sarney, S. P. Svensson, *Appl. Phys. Lett.* **2016**, *108*, 222101.
- [50] D. Z. Ting, A. Khoshakhlagh, A. Soibel, S. D. Gunapala, *J. Elec. Mater.* **2020**, *49*, 6936.
- [51] D. Z. Ting, A. Soibel, S. D. Gunapala, *Appl. Phys. Lett.* **2016**, *108*, 183504.
- [52] D. Z. Ting, A. Soibel, S. D. Gunapala, *Infrared Phys. Technol.* **2017**, *84*, 102.
- [53] P. C. Klipstein, E. Avnon, Y. Benny, R. Fraenkel, A. Glozman, S. Grossman, O. Klin, L. Langoff, Y. Livneh, I. Lukomsky, M. Nitzani, L. Shkedy, I. Shtrichman, N. Snapi, A. Tuito, E. Weiss, *Proc. SPIE* **2014**, 9070, 90700U.
- [54] N. A. Kotulak, J. A. Nolde, M. B. Katz, M. E. Twigg, K. E. Knipling, D. Lubyshev, J. M. Fastenau, A. W. K. Liu, E. H. Aifer, *J. Appl. Phys.* **2020**, *128*, 015302.
- [55] H. J. Haugan, K. Mahalingam, F. Szmulowicz, G. J. Brown, *J. Cryst. Growth* **2016**, *436*, 134.
- [56] Y. Livneh, P. C. Klipstein, O. Klin, N. Snapi, S. Grossman, A. Glozman, E. Weiss, *Phys. Rev. B* **2012**, *86*, 235311.
- [57] D. Z. Ting, S. B. Rafol, S. A. Keo, J. Nguyen, A. Khoshakhlagh, A. Soibel, L. Höglund, A. M. Fisher, E. M. Luong, J. M. Mumolo, J. K. Liu, S. D. Gunapala, *IEEE Photonics J.* **2018**, *10*, 1.
- [58] D. Donetsky, S. P. Svensson, L. E. Vorobjev, G. Belenky, *Appl. Phys. Lett.* **2009**, *95*, 212104.
- [59] B. C. Connelly, G. D. Metcalfe, H. Shen, M. Wraback, *Proc. SPIE* **2013**, 8704, 87040V.
- [60] J. Steinshnider, M. Weimer, R. Kaspi, G. W. Turner, *Phys. Rev. Lett.* **2000**, *85*, 2953.
- [61] J. Steinshnider, J. Harper, M. Weimer, C.-H. Lin, S. S. Pei, D. H. Chow, *Phys. Rev. Lett.* **2000**, *85*, 4562.
- [62] S. P. Svensson, D. Donetsky, D. Wang, H. Hier, F. J. Crowne, G. Belenky, *J. Cryst. Growth* **2011**, *334*, 103.
- [63] S.-H. Wei, A. Zunger, *Phys. Rev. B* **1995**, *52*, 12039.
- [64] G. S. Lee, Y. Lo, Y. F. Lin, S. M. Bedair, W. D. Laidig, *Appl. Phys. Lett.* **1985**, *47*, 1219.
- [65] L. R. Dawson, *J. Vac. Sci. Technol. B* **1986**, *4*, 598.
- [66] M. Kopytko, E. Gornóka, T. Manyk, K. Michalczewski, Ł. Kubiszyn, J. Rutkowski, P. Martyniuk, *Adv. Infrared Technol. Appl.* **2019**, *27*, 37.
- [67] D. Z. Ting, A. Soibel, A. Khoshakhlagh, S. A. Keo, S. B. Rafol, A. M. Fisher, B. J. Pepper, E. M. Luong, C. J. Hill, S. D. Gunapala, *Infrared Phys. Technol.* **2019**, *97*, 210.
- [68] C. Cervera, K. Jaworowicz, H. Ait-Kaci, R. Chaghi, J. B. Rodriguez, I. Ribet-Mohamed, P. Christol, *Infrared Phys. Technol.* **2011**, *54*, 258.

- [69] Y. Aytac, B. V. Olson, J. K. Kim, E. A. Shaner, S. D. Hawkins, J. F. Klem, J. Olesberg, M. E. Flatté, T. F. Boggess, *J. Appl. Phys.* **2016**, *119*, 215705.
- [70] Y. Aytac, B. V. Olson, J. K. Kim, E. A. Shaner, S. D. Hawkins, J. F. Klem, M. E. Flatté, T. F. Boggess, *Appl. Phys. Lett.* **2014**, *105*, 022107.
- [71] B. Klein, N. Gautam, E. Plis, T. Schuler-Sandy, T. J. Rotter, S. Krishna, B. C. Connelly, G. D. Metcalfe, P. Shen, M. Wraback, *J. Vac. Sci. Technol. B* **2014**, *32*, 02C101.
- [72] Y. Aytac, B. V. Olson, J. K. Kim, E. A. Shaner, S. D. Hawkins, J. F. Klem, M. E. Flatté, T. F. Boggess, *Proc. SPIE* **2015**, 9370, 93700J.
- [73] Z.-Y. Lin, S. Liu, E. H. Steenbergen, Y.-H. Zhang, *Appl. Phys. Lett.* **2015**, *107*, 201107.
- [74] E. H. Steenbergen, J. A. Massengale, G. Ariyawansa, Y.-H. Zhang, *J. Lumin.* **2016**, *178*, 451.
- [75] B. C. Connelly, G. D. Metcalfe, H. Shen, M. Wraback, C. L. Canedy, I. Vurgaftman, J. S. Melinger, C. A. Affouda, E. M. Jackson, J. A. Nolde, J. R. Meyer, E. H. Aifer, *J. Elect. Mater.* **2013**, *42*, 3203.
- [76] G. Jenkins, PhD Thesis, The University of New Mexico, **2018**.
- [77] C. N. Kadlec, E. S. Bielejec, M. Goldflam, E. A. Kadlec, E. M. Anderson, E. A. Shaner, J. K. Kim, P. A. Schultz, J. F. Klem, S. D. Hawkins, presented at the Hardened Elec. Rad. Technol. Conf. In-Situ Annealing Studies of Radiation Induced Defects in InAs/InAsSb Type-II Superlattices under Ion Irradiation, Tucson, Arizona, USA, April 2018.
- [78] Z. Lin, PhD Thesis, Arizona State University, **2016**.
- [79] C. N. Kadlec, E. A. Kadlec, M. Goldflam, E. S. Bielejec, J. K. Kim, B. V. Olson, J. F. Klem, S. D. Hawkins, J. E. Moussa, P. A. Schultz, C. P. Morath, G. D. Jenkins, V. M. Cowan, E. A. Shaner, presented at the SPIE Optics and Photonics Conf. Effects of 4.5 MeV and 63 MeV Proton Irradiation on Carrier Lifetime of InAs/InAsSb Type-II Superlattices, San Diego, CA, August 2017.
- [80] L. Höglund, D. Z. Ting, A. Soibel, A. Fisher, A. Khoshakhlagh, C. J. Hill, S. Keo, S. D. Gunapala, *Appl. Phys. Lett.* **2014**, *105*, 193510.
- [81] Z.-Y. Lin, J. Fan, S. Liu, Y.-H. Zhang, *Proc. SPIE* **2015**, 9451, 94510Q.
- [82] U. Zavala-Moran, M. Bouschet, J. P. Perez, R. Alchaar, S. Bernhardt, I. Ribet-Mohamed, F. de Anda-Salazar, P. Christol, *Photonics* **2020**, *7*, 76.
- [83] A. Soibel, D. Z. Ting, S. B. Rafol, A. M. Fisher, S. A. Keo, A. Khoshakhlagh, S. D. Gunapala, *Appl. Phys. Lett.* **2019**, *114*, 161103.
- [84] S. P. Svensson, D. Donetsky, D. Wang, P. Maloney, G. Belenky, *Proc. SPIE* **2010**, 7660, 76601V.
- [85] Z. Taghipour, S. Lee, S. A. Myers, E. H. Steenbergen, C. P. Morath, V. M. Cowan, S. Mathews, G. Balakrishnan, S. Krishna, *Phys. Rev. Appl.* **2019**, *11*, 024047.
- [86] Z. Taghipour, E. H. Steenbergen, S. I. Maximenko, C. P. Morath, V. M. Cowan, S. Mathews, E. H. Aifer, G. Balakrishnan, S. Krishna, *Proc. SPIE* **2018**, 10624, 106240N.
- [87] Z. Taghipour, A. Kazemi, S. Myers, P. Wijewarnasuriya, S. Mathews, E. H. Steenbergen, C. Morath, V. M. Cowan, G. Ariyawansa, J. Scheihing, S. Krishna, *Proc. SPIE* **2017**, 10404, 1040406.
- [88] B. C. Connelly, G. D. Metcalfe, H. Shen, M. Wraback, *Proc. SPIE* **2011**, 8155, 81550L.
- [89] Y. Chang, J. Zhao, H. Abad, C. H. Grein, S. Sivananthan, T. Aoki, D. J. Smith, *Appl. Phys. Lett.* **2005**, *86*, 131924.
- [90] I. Madni, G. A. Umana-Membreno, W. Lei, R. Gu, J. Antoszewski, L. Faraone, *Appl. Phys. Lett.* **2015**, *107*, 182107.
- [91] G. Belenky, D. Donetsky, G. Kipshidze, D. Wang, L. Shterengas, W. L. Sarney, S. P. Svensson, *Appl. Phys. Lett.* **2011**, *99*, 141116.
- [92] Z. Taghipour, V. Dahiya, T. Grassman, J. M. Fastenau, A. W. K. Liu, D. Lubyshev, S. Krishna, *Proc. SPIE* **2019**, 11129, 1112905.
- [93] N. Baril, A. Brown, D. Zuo, M. Tidrow, D. Loubychev, J. M. Fastenau, A. W. K. Liu, S. Bandara, *Proc. SPIE* **2017**, 10177, 101771L.
- [94] Y. Lin, PhD Thesis, Stony Brook University, **2016**.
- [95] D. Wang, Y. Lin, D. Donetsky, L. Shterengas, G. Kipshidze, G. Belenky, W. L. Sarney, H. Hier, S. P. Svensson, *Proc. SPIE* **2012**, 8353, 835312.
- [96] Y. Dong, Master Thesis, George Mason University, **2017**.
- [97] X. Li, Y. Zhang, D. Jiang, F. Guo, D. Wang, L. Zhao, *Superlattices Microstruct.* **2017**, *104*, 390.
- [98] Y. Ashuach, Y. Kauffmann, D. Isheim, Y. Amouyal, D. N. Seidman, E. Zolotoyabko, *Appl. Phys. Lett.* **2012**, *100*, 241604.
- [99] M. E. Twigg, B. R. Bennett, P. M. Thibado, B. V. Shanabrook, L. J. Whitman, *Philos. Mag. A* **1998**, *77*, 7.
- [100] E. Plis, S. Annamalai, K. T. Posani, S. Krishna, R. A. Rupani, S. Ghosh, *J. Appl. Phys.* **2006**, *100*, 014510.
- [101] S. Cervera, J. B. Rodriguez, R. Chaghi, H. Ait-Kaci, P. Christol, *J. Appl. Phys.* **2009**, *106*, 024501.
- [102] J. B. Rodriguez, P. Christol, L. Cerutti, F. Chevrier, A. Joullié, *J. Cryst. Growth* **2005**, *274*, 6.
- [103] M. Seta, H. Asahi, S. G. Kim, K. Asami, S. Gonda, *J. Appl. Phys.* **1993**, *74*, 5033.
- [104] N. Herres, F. Fuchs, J. Schmitz, K. M. Pavlov, J. Wagner, J. D. Ralston, P. Koidl, C. Gadaleta, G. Scamarcio, *Phys. Rev. B* **1996**, *53*, 15688.
- [105] D. H. Tomich, W. C. Mitchel, P. Chow, C. W. Tu, *J. Cryst. Growth* **1999**, *201*, 868.
- [106] X. Li, Y. Zhao, Q. Wu, Y. Teng, X. Hao, Y. Huang, *J. Cryst. Growth* **2018**, *502*, 71.
- [107] Y. Chen, J. Liu, Y. Zhao, Y. Teng, X. Hao, X. Li, H. Zhu, H. Zhu, Q. Wu, Y. Huang, *Infrared Phys. Technol.* **2020**, *105*, 103209.
- [108] Z. Deng, D. Guo, C. G. Burgette, Z. Xie, J. Huang, H. Liu, J. Wu, B. Chen, *Infrared Phys. Technol.* **2019**, *101*, 133.
- [109] J. Guo, H. Chen, W. Sun, R. Hao, Y. Xu, Z. Niu, *Sci. China Ser. E-Technol. Sci.* **2009**, *52*, 23.
- [110] Y. Liu, C. Zhang, X. Wang, J. Wu, L. Huang, *Infrared Phys. Technol.* **2020**, *113*, 103573.
- [111] M. Delmas, M. C. Debnath, B. L. Liang, D. L. Huffaker, *Infrared Phys. Technol.* **2018**, *94*, 286.
- [112] M. Kesaria, D. Alshahrani, D. Kwan, E. Anyebe, V. Srivastava, *Mater. Res. Bull.* **2021**, *142*, 111424.
- [113] G. Jie, S. Wei-Guo, P. Zhen-Yu, Z. Zhi-Qiang, X. Ying-Qiang, N. Zhi-Chuan, *Chinese Phys. Lett.* **2009**, *26*, 047802.
- [114] J. Lu, E. Luna, T. Aoki, E. H. Steenbergen, Y.-H. Zhang, D. J. Smith, *J. Appl. Phys.* **2016**, *119*, 095702.
- [115] H. J. Haugan, F. Szmulowicz, J. J. Hudgins, L. E. Cordonnier, G. J. Brown, *Proc. SPIE* **2017**, 10404, 104040W.
- [116] J.-K. Jiang, Y. Li, F.-R. Chang, S.-N. Cui, W.-Q. Chen, D.-W. Jiang, G.-W. Wang, Y.-Q. Xu, Z.-C. Niu, R. Che, C. Zhang, L. Huang, *J. Cryst. Growth* **2021**, *564*, 126109.
- [117] R. M. Biefeld, *Mater. Sci. Eng. R Rep.* **2002**, *36*, 105.
- [118] M. Razeghi, A. Dehzangi, D. Wu, R. McClintock, Y. Zhang, Q. Durlin, J. Li, F. Meng, *Proc. SPIE* **2019**, 11002, 110020G.
- [119] R. Hao, Y. Xu, Z. Zhou, Z. Ren, H. Ni, Z. He, Z. Niu, *J. Phys. D: Appl. Phys.* **2007**, *40*, 6690.
- [120] D. Lubyshev, J. M. Fastenau, Y. Qiu, A. W. K. Liu, E. J. Koerperick, J. T. Olesberg, D. Norton Jr., N. N. Faleev, C. B. Honsberg, *Proc. SPIE* **2013**, 8704, 870412.
- [121] H. Ruiting, X. Yingqiang, Z. Zhiqiang, R. Zhengwei, N. Zhichuan, *J. Semicond.* **2007**, *28*, 1088.
- [122] A. Jasik, I. Sankowska, J. Ratajczak, A. Wawro, D. Smoczyński, K. Czuba, M. Wzorek, *Curr. Appl. Phys.* **2019**, *19*, 120.
- [123] B. V. Olson, J. K. Kim, E. A. Kadlec, J. F. Klem, S. D. Hawkins, W. T. Coon, T. R. Fortune, A. Tauke-Pedretti, M. A. Cavaliere, E. A. Shaner, *Appl. Phys. Lett.* **2016**, *108*, 252104.
- [124] Y. Huang, J.-H. Ryou, R. D. Dupuis, A. Petschke, M. Mandl, S.-L. Chuang, *Appl. Phys. Lett.* **2010**, *96*, 251107.

- [125] X. B. Zhang, J. H. Ryou, R. D. Dupuis, A. Petschke, S. Mou, S. L. Chuang, C. Xu, K. C. Hsieh, *Appl. Phys. Lett.* **2006**, *88*, 072104.
- [126] X. B. Zhang, J. H. Ryou, R. D. Dupuis, C. Xu, S. Mou, A. Petschke, K. C. Hsieh, S. L. Chuang, *Appl. Phys. Lett.* **2007**, *90*, 131110.
- [127] P. Barletta, G. Bulman, G. Dezzi, R. Venkatasubramanian, *Thin Solid Films* **2012**, *520*, 2170.
- [128] S. Arikata, T. Kyono, K. Miura, S. Balasekaran, H. Inada, Y. Iguchi, M. Sakai, H. Katayama, M. Kimata, K. Akita, *Phys. Status Solidi A* **2017**, *214*, 1600582.
- [129] D. Wu, A. Dehzangi, M. Razeghi, *Appl. Phys. Lett.* **2019**, *115*, 061102.
- [130] D. Wu, A. Dehzangi, J. Li, M. Razeghi, *Appl. Phys. Lett.* **2020**, *116*, 161108.
- [131] X. Li, J. Cui, Y. Zhao, Q. Wu, Y. Teng, X. Hao, Y. Chen, J. Liu, H. Zhu, Y. Huang, Y. Yao, *J. Appl. Phys.* **2020**, *127*, 045305.
- [132] L.-G. Li, S.-M. Liu, S. Luo, T. Yang, L.-J. Wang, J.-Q. Liu, F.-Q. Liu, X.-L. Ye, B. Xu, Z.-G. Wang, *J. Cryst. Growth* **2012**, *359*, 55.
- [133] Z.-D. Ning, S.-M. Liu, S. Luo, F. Ren, F.-J. Wang, T. Yang, F.-Q. Liu, Z.-G. Wang, L.-C. Zhao, *Appl. Surf. Sci.* **2016**, *368*, 110.
- [134] E. H. Steenbergen, Y. Huang, J.-H. Ryou, L. Ouyang, J.-J. Li, D. J. Smith, R. D. Dupuis, Y.-H. Zhang, *Appl. Phys. Lett.* **2011**, *99*, 071111.
- [135] L. Ouyang, E. H. Steenbergen, O. O. Cellek, Y.-H. Zhang, D. J. Smith, *Proc. SPIE* **2012**, *8268*, 826830.
- [136] Y. Teng, Y. Zhao, Q. Wu, X. Li, X. Hao, M. Xiong, Y. Huang, *IEEE Photonics Technol. Lett.* **2019**, *31*, 185.
- [137] Y. Zhao, Y. Teng, X. Hao, Q. Wu, J. Miao, X. Li, M. Xiong, Y. Huang, *IEEE Photonics Technol. Lett.* **2020**, *32*, 19.
- [138] H. Zhu, X. Hao, Y. Teng, J. Liu, H. Zhu, M. Li, Y. Huai, Y. Huang, *IEEE Photonics Technol. Lett.* **2021**, *33*, 429.
- [139] J. Liu, Y. Teng, X. Hao, Y. Zhao, Q. Wu, X. Li, H. Zhu, Y. Chen, R. Huang, S. Ding, Y. Huang, *IEEE J. Quantum Electron.* **2020**, *56*, 1.
- [140] B. Streetman, S. Banerjee, *Solid State Electronic Devices*, Pearson, Boston **2014**.
- [141] H. Katayama, T. Takekawa, M. Kimata, H. Inada, Y. Iguchi, *Infrared Phys. Technol.* **2015**, *70*, 53.
- [142] V. Letka, J. Keen, A. Craig, A. R. J. Marshall, *Proc. SPIE* **2017**, *10433*, 1043319.
- [143] M. E. Flatté, C. H. Grein, *Proc. SPIE* **2015**, *9370*, 93700K.
- [144] G. Deng, X. Song, M. Fan, T. Xiao, Z. Luo, N. Chen, W. Yang, Y. Zhang, *Opt. Express* **2020**, *28*, 13616.
- [145] D. Wu, J. Li, A. Dehzangi, M. Razeghi, *Infrared Phys. Technol.* **2020**, *109*, 103439.
- [146] G. Deng, D. Chen, S. Yang, C. Yang, J. Yuan, W. Yang, Y. Zhang, *Opt. Express* **2020**, *28*, 17611.
- [147] D. Lubyshev, J. M. Fastenau, M. Kattner, P. Frey, S. A. Nelson, R. Flick, M. Rogers, A. W. K. Liu, P. Flint, N. Faleev, *Infrared Phys. Technol.* **2018**, *95*, 27.
- [148] G. Ariyawansa, J. Duran, C. Reyner, J. Scheihing, *Micromachines* **2019**, *10*, 806.
- [149] A. Haddadi, M. Razeghi, *Opt. Lett.* **2017**, *42*, 4275.
- [150] A. M. Hoang, G. Chen, A. Haddadi, M. Razeghi, *Appl. Phys. Lett.* **2013**, *102*, 011108.
- [151] C. Asplund, R. Marcks von Würtemberg, D. Lantz, H. Malm, H. Martijn, E. Plis, N. Gautam, S. Krishna, *Infrared Phys. Technol.* **2013**, *59*, 22.
- [152] G. Chen, B.-M. Nguyen, A. M. Hoang, E. K. Huang, S. R. Darvish, M. Razeghi, *Proc. SPIE* **2012**, *8268*, 826811.
- [153] A. Rogalski, P. Martyniuk, M. Kopytko, *Appl. Phys. Rev.* **2017**, *4*, 031304.
- [154] P. C. Klipstein, Y. Benny, S. Gliksman, A. Glozman, E. Hojman, O. Klin, L. Langof, I. Lukomsky, I. Marderfeld, M. Nitzani, N. Snapi, E. Weiss, *Infrared Phys. Technol.* **2019**, *96*, 155.
- [155] K. Czuba, I. Sankowska, J. Jureńczyk, A. Jasik, E. Papis-Polakowska, J. Kaniewski, *Semicond. Sci. Technol.* **2017**, *32*, 055010.
- [156] S. Bandara, P. G. Maloney, N. Baril, J. G. Pellegrino, M. Z. Tidrow, *Opt. Eng.* **2011**, *50*, 061015.
- [157] E. A. Kadlec, B. V. Olson, M. D. Goldflam, J. K. Kim, J. F. Klem, S. D. Hawkins, W. T. Coon, M. A. Cavaliere, A. Tauke-Pedretti, T. R. Fortune, C. T. Harris, E. A. Shaner, *Appl. Phys. Lett.* **2016**, *109*, 261105.
- [158] B. C. Connelly, G. D. Metcalfe, H. Shen, M. Wraback, *Appl. Phys. Lett.* **2010**, *97*, 251117.
- [159] R. C. Jones, *Rev. Sci. Instrum.* **1953**, *24*, 1035.
- [160] A. Haddadi, R. Chevallier, G. Chen, A. M. Hoang, M. Razeghi, *Appl. Phys. Lett.* **2015**, *106*, 011104.
- [161] A. Dehzangi, D. Wu, R. McClintock, J. Li, M. Razeghi, *Appl. Phys. Lett.* **2020**, *116*, 221103.
- [162] D. Wu, J. Li, A. Dehzangi, M. Razeghi, *AIP Adv.* **2020**, *10*, 025018.
- [163] E. Delli, V. Letka, P. D. Hodgson, E. Repiso, J. P. Hayton, A. P. Craig, Q. Lu, R. Beanland, A. Krier, A. R. J. Marshall, P. J. Carrington, *ACS Photonics* **2019**, *6*, 538.
- [164] J. Kim, H. Yuan, J. Kimchi, J. Lei, E. Rangel, P. Dreiske, A. Ikhlasi, *Proc. SPIE* **2018**, *10624*, 1062412.
- [165] J. Kim, H. Yuan, A. Rumyantsev, P. Bey, D. Bond, J. Kimchi, M. G. DeForest, *Proc. SPIE* **2020**, *11276*, 112760J.
- [166] D. Z. Ting, A. Soibel, A. Khoshakhlagh, S. B. Rafol, S. A. Keo, L. Höglund, A. M. Fisher, E. M. Luong, S. D. Gunapala, *Appl. Phys. Lett.* **2018**, *113*, 021101.
- [167] D. Wu, Q. Durlin, A. Dehzangi, Y. Zhang, M. Razeghi, *Appl. Phys. Lett.* **2019**, *114*, 011104.
- [168] E. Plis, J. B. Rodriguez, G. Balakrishnan, Y. D. Sharma, H. S. Kim, T. Rotter, S. Krishna, *Semicond. Sci. Technol.* **2010**, *25*, 085010.
- [169] D. A. Ramirez, E. A. Plis, S. Myers, L. A. Treider, E. Garduno, C. P. Morath, V. M. Cowan, S. Krishna, *Proc. SPIE* **2014**, *9226*, 92260Q.
- [170] N. Gautam, S. Myers, A. V. Barve, B. Klein, E. P. Smith, D. R. Rhiger, H. S. Kim, Z.-B. Tian, S. Krishna, *IEEE J. Quantum Electron.* **2013**, *49*, 211.
- [171] Z. Deng, D. Guo, J. Huang, H. Liu, J. Wu, B. Chen, *IEEE J. Quantum Electron.* **2019**, *55*, 1.
- [172] G. Bishop, E. Plis, J. B. Rodriguez, Y. D. Sharma, H. S. Kim, L. R. Dawson, S. Krishna, *J. Vac. Sci. Technol. B* **2008**, *26*, 1145.
- [173] Y. Shi, R. Hu, G. Deng, W. He, J. Feng, M. Fang, X. Li, J. Deng, *Proc. SPIE* **2015**, *9451*, 94510L.
- [174] P. Martyniuk, J. Wróbel, E. Plis, P. Madejczyk, A. Kowalewski, W. Gawron, S. Krishna, A. Rogalski, *Semicond. Sci. Technol.* **2012**, *27*, 055002.
- [175] J. Huang, Z. Xie, Y. Chen, J. Bowers, B. Chen, *IEEE J. Quantum Electron.* **2020**, *56*, 1.
- [176] S. A. Pour, E. K. Huang, G. Chen, A. Haddadi, B.-M. Nguyen, M. Razeghi, *Appl. Phys. Lett.* **2011**, *98*, 143501.
- [177] B.-M. Nguyen, D. Hoffman, E. K. Huang, S. Bogdanov, P.-Y. Delaunay, M. Razeghi, M. Z. Tidrow, *Appl. Phys. Lett.* **2009**, *94*, 223506.
- [178] E. Plis, J. B. Rodriguez, H. S. Kim, G. Bishop, Y. D. Sharma, L. R. Dawson, S. Krishna, S. J. Lee, C. E. Jones, V. Gopal, *Appl. Phys. Lett.* **2007**, *91*, 133512.
- [179] M. Korkmaz, B. Arian, Y. E. Suyolcu, B. Aslan, U. Serincan, *Semicond. Sci. Technol.* **2018**, *33*, 035002.
- [180] T. Tansel, M. Hostut, Y. Ergun, *Superlattices Microstruct.* **2017**, *111*, 1211.
- [181] Y. Wei, A. Hood, H. Yau, A. Gin, M. Razeghi, M. Z. Tidrow, V. Nathan, *Appl. Phys. Lett.* **2005**, *86*, 233106.
- [182] P. Martyniuk, D. Benyahia, A. Kowalewski, Ł. Kubiszyn, D. Stępień, W. Gawron, A. Rogalski, *Solid-State Electron.* **2016**, *119*, 1.

- [183] J. B. Rodriguez, E. Plis, G. Bishop, Y. D. Sharma, H. Kim, L. R. Dawson, S. Krishna, *Appl. Phys. Lett.* **2007**, *91*, 043514.
- [184] C. Guo, Z. Jiang, D. Jiang, G. Wang, Y. Xu, T. Wang, J. Tian, Z. Wu, Z. Niu, *Opt. Quantum Electron.* **2019**, *51*, 73.
- [185] H. Hao, W. Xiang, G. Wang, D. Jiang, Y. Xu, Z. Ren, Z. He, Z. Niu, *Proc. SPIE* **2014**, *9300*, 93001K.
- [186] M. Herrera, M. Chi, M. Bonds, N. D. Browning, J. N. Woolman, R. E. Kvaas, S. F. Harris, D. R. Rhiger, C. J. Hill, *Appl. Phys. Lett.* **2008**, *93*, 093106.
- [187] A. Hood, Y. Wei, A. Gin, M. Razeghi, M. Z. Tidrow, V. Nathan, *Proc. SPIE* **2005**, *5732*, 316.
- [188] M. Narayanan Kuttly, PhD Thesis, The University of New Mexico, **2013**.
- [189] O. Salihoglu, A. Muti, K. Kutluer, T. Tansel, R. Turan, C. Kocabas, A. Aydinli, *Proc. SPIE* **2012**, *8353*, 83530Z.
- [190] S. Maimon, G. W. Wicks, *Appl. Phys. Lett.* **2006**, *89*, 151109.
- [191] D. Zuo, R. Liu, D. Wasserman, J. Mabon, Z.-Y. He, S. Liu, Y.-H. Zhang, E. A. Kadlec, B. V. Olson, E. A. Shaner, *Appl. Phys. Lett.* **2015**, *106*, 071107.
- [192] U. Zavala-Moran, R. Alchaar, J. Perez, J. Rodriguez, M. Bouschet, V. Compean, F. de Anda, P. Christol, in *Proc. of the 8th Int. Conf. on Photonics, Opt. Laser Technol.*, Valletta, Malta **2020**, pp. 45–51.
- [193] A. Kazemi, S. Myers, Z. Taghipour, S. Mathews, T. Schuler-Sandy, S. Lee, V. M. Cowan, E. Garduno, E. Steenbergen, C. Morath, G. Ariyawansa, J. Scheihing, S. Krishna, *Infrared Phys. Technol.* **2018**, *88*, 114.
- [194] G. Chen, A. Haddadi, A.-M. Hoang, R. Chevallier, M. Razeghi, *Opt. Lett.* **2015**, *40*, 45.
- [195] J. Huang, W. Ma, Y. Zhang, Y. Cao, W. Huang, C. Zhao, *IEEE Electron Device Lett.* **2017**, *38*, 1266.
- [196] D. Z. Ting, A. Soibel, J. Nguyen, L. Höglund, A. Khoshakhlagh, S. B. Rafol, S. A. Keo, A. Liao, J. M. Mumolo, J. K. Liu, S. D. Gunapala, *Proc. SPIE* **2011**, *8154*, 81540L.
- [197] M. Razeghi, *Proc. SPIE* **2020**, *11407*, 114070T.
- [198] B.-M. Nguyen, M. Razeghi, V. Nathan, G. J. Brown, *Proc. SPIE* **2007**, *6479*, 64790S.
- [199] C. L. Canedy, E. H. Aifer, J. H. Warner, I. Vurgaftman, E. M. Jackson, J. G. Tischler, S. P. Powell, K. Olver, J. R. Meyer, W. E. Tennant, *Infrared Phys. Technol.* **2009**, *52*, 326.
- [200] O. Salihoglu, A. Muti, K. Kutluer, T. Tansel, R. Turan, Y. Ergun, A. Aydinli, *Appl. Phys. Lett.* **2012**, *101*, 073505.
- [201] A. Kilic, T. Tansel, M. Hostut, S. Elagoz, Y. Ergun, *Semicond. Sci. Technol.* **2018**, *33*, 094001.
- [202] T. Tansel, M. Hostut, S. Elagoz, A. Kilic, Y. Ergun, A. Aydinli, *Superlattices Microstruct.* **2016**, *91*, 1.
- [203] P. Martyniuk, K. Michalczewski, T. Y. Tsai, C.-H. Wu, Y.-R. Wu, *Compd. Semicond. Week CSW*, **2019**, *1*.
- [204] P. Martyniuk, K. Michalczewski, T.-Y. Tsai, C.-H. Wu, Y.-R. Wu, *Phys. Status Solidi A* **2020**, *217*, 1900522.
- [205] A. Manissadjian, L. Rubaldo, Y. Rebeil, A. Kerlain, D. Brellier, L. Mollard, *Proc. SPIE* **2012**, *8353*, 835334.
- [206] D. Z. Ting, A. Soibel, A. Khoshakhlagh, S. A. Keo, S. B. Rafol, L. Höglund, E. M. Luong, A. M. Fisher, C. J. Hill, S. D. Gunapala, *J. Electron. Mater.* **2019**, *48*, 6145.
- [207] D. Z.-Y. Ting, C. J. Hill, A. Soibel, S. A. Keo, J. M. Mumolo, J. Nguyen, S. D. Gunapala, *Appl. Phys. Lett.* **2009**, *95*, 023508.
- [208] V. M. More, Y. Kim, J. Jeon, J. C. Shin, S. J. Lee, *J. Alloy. Compd.* **2021**, *868*, 159195.
- [209] A. Haddadi, A. Dehzangi, R. Chevallier, S. Adhikary, M. Razeghi, *Sci. Rep.* **2017**, *7*, 3379.
- [210] X. Ma, J. Guo, R. Hao, G. Wei, F. Chang, Y. Li, X. Li, D. Jiang, D. Jiang, G. Wang, G. Wang, Y. Xu, Y. Xu, Z. Niu, Z. Niu, *Opt. Mater. Express* **2021**, *11*, 585.
- [211] M. Razeghi, A. Dehzangi, J. Li, (Preprint) *ResearchGate*, **2020**, <https://doi.org/10.13140/RG.2.2.31911.78240>.
- [212] P. Martyniuk, J. Antoszewski, M. Martyniuk, L. Faraone, A. Rogalski, *Appl. Phys. Rev.* **2014**, *1*, 041102.
- [213] M. Razeghi, *Mid-Infrared Optoelectronics Materials, Devices, and Applications*, Woodhead Publishing, **2020**.
- [214] P. C. Klipstein, *J. Cryst. Growth* **2015**, *425*, 351.
- [215] R. Taalat, J.-B. Rodriguez, M. Delmas, P. Christol, *J. Appl. Phys.* **2013**, *47*, 015101.
- [216] E. Giard, I. Ribet-Mohamed, J. Jaeck, T. Viale, R. Haïdar, R. Taalat, M. Delmas, J.-B. Rodriguez, E. Steveler, N. Bardou, F. Boulard, P. Christol, *J. Appl. Phys.* **2014**, *116*, 043101.
- [217] J. Nghiem, E. Giard, M. Delmas, J. B. Rodriguez, P. Christol, M. Caes, H. Martijn, E. Costard, I. Ribet-Mohamed, *Proc. SPIE* **2017**, *10562*, 105623Y.
- [218] P. Christol, J.-B. Rodriguez, *Proc. SPIE* **2017**, *10563*, 105632C.
- [219] J. Schmidt, F. Rutz, A. Wörl, V. Daumer, R. Rehm, *Infrared Phys. Technol.* **2017**, *85*, 378.
- [220] T. Schuler-Sandy, S. Myers, B. Klein, N. Gautam, P. Ahirwar, Z.-B. Tian, T. Rotter, G. Balakrishnan, E. Plis, S. Krishna, *Appl. Phys. Lett.* **2012**, *101*, 071111.
- [221] R. Hao, Y. Ren, S. Liu, J. Guo, G. Wang, Y. Xu, Z. Niu, *J. Cryst. Growth* **2017**, *470*, 33.
- [222] Yang Ren, *Chin. Phys. Lett.* **2016**, *33*, 128101.
- [223] D. R. Rhiger, E. P. Smith, B. P. Kolasa, J. K. Kim, J. F. Klem, S. D. Hawkins, *J. Elec. Materi.* **2016**, *45*, 4646.
- [224] Q. Durlin, J. P. Perez, L. Cerutti, J. B. Rodriguez, T. Cerba, T. Baron, E. Tournié, P. Christol, *Infrared Phys. Technol.* **2019**, *96*, 39.
- [225] T. Schuler-Sandy, B. Klein, L. Casias, S. Mathews, C. Kadlec, Z. Tian, E. Plis, S. Myers, S. Krishna, *J. Cryst. Growth* **2015**, *425*, 29.
- [226] L. Höglund, C. Asplund, R. Marcks von Würtemberg, H. Kataria, A. Gamfeldt, S. Smuk, H. Martijn, E. Costard, *Infrared Phys. Technol.* **2017**, *84*, 28.
- [227] V. Daumer, V. Gramich, R. Müller, J. Schmidt, F. Rutz, T. Stadelmann, A. Wörl, R. Rehm, *Proc. SPIE* **2017**, *10177*, 1017711.
- [228] H. J. Lee, S. Y. Ko, Y. H. Kim, J. Nah, *J. Semicond.* **2020**, *41*, 062302.
- [229] R. Taalat, J. B. Rodriguez, C. Cervera, I. Ribet-Mohamed, P. Christol, *Infrared Phys. Technol.* **2013**, *59*, 32.
- [230] J. Chen, Y. Zhou, Z. Xu, J. Xu, Q. Xu, H. Chen, L. He, *J. Cryst. Growth* **2013**, *378*, 596.
- [231] K. Jaworowicz, C. Cervera, O. Gravrand, J.-B. Rodriguez, P. Christol, I. Ribet-Mohamed, *Proc. SPIE* **2010**, *7608*, 76081T.
- [232] Q. Li, W. Ma, Y. Zhang, K. Cui, J. Huang, Y. Wei, K. Liu, Y. Cao, W. Wang, Y. Liu, P. Jin, *Chin. Sci. Bull.* **2014**, *59*, 3696.
- [233] I. Ribet-Mohamed, M. Tauvy, R. Taalat, C. Cervera, J.-B. Rodriguez, P. Christol, *Proc. SPIE* **2012**, *8268*, 826833.
- [234] O. Salihoglu, A. Muti, A. Aydinli, *IEEE J. Quantum Electron.* **2013**, *49*, 661.
- [235] H. S. Kim, *J. Korean Phys. Soc.* **2020**, *77*, 714.
- [236] L. Zhang, W. Sun, Y. Xu, L. Zhang, L. Zhang, J. Si, *Infrared Phys. Technol.* **2014**, *65*, 129.
- [237] G. Wang, W. Xiang, Y. Xu, L. Zhang, Z. Peng, Y. Lü, J. Si, J. Wang, J. Xing, Z. Ren, Z. Niu, *J. Semicond.* **2013**, *34*, 114012.
- [238] P. J. Carrington, E. Delli, V. Letka, M. Bentley, P. D. Hodgson, E. Repiso, J. P. Hayton, A. P. Craig, Q. Lu, R. Beanland, A. Krier, A. R. J. Marshall, *Proc. SPIE* **2020**, *11503*, 115030G.
- [239] E. Plis, S. Annamalai, K. T. Posani, S. J. Lee, S. Krishna, *Proc. SPIE* **2006**, *6206*, 62060O.
- [240] P. Klipstein, *Proc. SPIE* **2008**, *6940*, 69402U.
- [241] P. C. Klipstein, Y. Gross, D. Aronov, M. ben Ezra, E. Berkowicz, Y. Cohen, R. Fraenkel, A. Glozman, S. Grossman, O. Klin, I. Lukomsky, T. Marlowitz, L. Shkedy, I. Shtrichman, N. Snapi, A. Tuito, M. Yassen, E. Weiss, *Proc. SPIE* **2013**, *8704*, 87041S.

- [242] M. Razeghi, S. A. Pour, E. Huang, G. Chen, A. Haddadi, B.-M. Nguyen, *Proc. SPIE* **2011**, 8012, 80122Q.
- [243] H. Sharifi, M. Roebuck, S. Terterian, J. Jenkins, B. Tu, W. Strong, T. J. D. Lyon, R. D. Rajavel, J. Caulfield, B. Z. Nosh, J. P. Curzan, *Proc. SPIE* **2017**, 10177, 101770U.
- [244] D. Z. Ting, A. Soibel, A. Khoshakhlagh, S. A. Keo, S. B. Rafol, A. M. Fisher, C. J. Hill, E. M. Luong, B. J. Pepper, S. D. Gunapala, *Proc. SPIE* **2019**, 11002, 110020F.
- [245] Y. Sun, X. Han, H. Hao, D. Jiang, C. Guo, Z. Jiang, Y. Lv, G. Wang, Y. Xu, Z. Niu, *Infrared Phys. Technol.* **2017**, 82, 140.
- [246] F. Oguz, Y. Arslan, E. Ulker, A. Bek, E. Ozbay, *IEEE J. Quantum Electron.* **2019**, 55, 1.
- [247] L. Höglund, R. M. von Würtemberg, C. Asplund, H. Kataria, A. Gamfeldt, E. Costard, *Proc. SPIE* **2017**, 10177, 1017713.
- [248] S. Gunapala, D. Ting, A. Soibel, A. Khoshakhlagh, S. Rafol, C. Hill, A. Fisher, B. Pepper, K.-K. Choi, A. D'Souza, C. Masterjohn, S. Babu, P. Ghuman, *Proc. SPIE* **2019**, 11180, 111803T.
- [249] S. Gunapala, S. Rafol, D. Ting, A. Soibel, A. Khoshakhlagh, S. Keo, B. Pepper, A. Fisher, C. Hill, K.-K. Choi, A. D'Souza, C. Masterjohn, S. Babu, P. Ghuman, *Proc. SPIE* **2019**, 11129, 111290C.
- [250] T. L. Haran, J. C. James, S. E. Lane, T. E. Cincotta, *Infrared Phys. Technol.* **2019**, 97, 309.
- [251] L. Höglund, C. Asplund, R. M. von Würtemberg, A. Gamfeldt, H. Kataria, D. Lantz, S. Smuk, E. Costard, H. Martijn, *Proc. SPIE* **2016**, 9819, 98190Z.
- [252] X. Zhou, D. Li, J. Huang, Y. Zhang, Y. Mu, W. Ma, X. Tie, D. Zuo, *Infrared Phys. Technol.* **2016**, 78, 263.
- [253] P.-Y. Delaunay, B. Z. Nosh, A. R. Gurga, S. Terterian, R. D. Rajavel, *Proc. SPIE* **2017**, 10177, 101770T.
- [254] D. Eich, W. Schirmacher, S. Hanna, K. M. Mahlein, P. Fries, H. Figgemeier, *J. Elect. Mater.* **2017**, 46, 5448.
- [255] R. Q. Yang, Z. Tian, Z. Cai, J. F. Klem, M. B. Johnson, H. C. Liu, *J. Appl. Phys.* **2010**, 107, 054514.
- [256] W. Huang, S. M. S. Rassel, L. Li, J. A. Massengale, R. Q. Yang, T. D. Mishima, M. B. Santos, *Infrared Phys. Technol.* **2019**, 96, 298.
- [257] N. Gautam, S. Myers, A. V. Barve, B. Klein, E. P. Smith, D. R. Rhiger, L. R. Dawson, S. Krishna, *Appl. Phys. Lett.* **2012**, 101, 021106.
- [258] Z.-B. Tian, S. E. Godoy, H. S. Kim, T. Schuler-Sandy, J. A. Montoya, S. Krishna, *Appl. Phys. Lett.* **2014**, 105, 051109.
- [259] Z.-B. Tian, S. Krishna, *IEEE J. Quantum Electron.* **2015**, 51, 1-5.
- [260] L. Lei, L. Li, H. Lotfi, H. Ye, R. Q. Yang, T. D. Mishima, M. B. Santos, M. B. Johnson, *Opt. Eng.* **2017**, 57, 011006.
- [261] Y. Zhou, J. Chen, Z. Xu, L. He, *Semicond. Sci. Technol.* **2016**, 31, 085005.
- [262] W. Pusz, A. Kowalewski, P. Martyniuk, W. Gawron, E. Plis, S. Krishna, A. Rogalski, *Opt. Eng.* **2014**, 53, 043107.
- [263] Y. Zhou, J. Chen, Z. Xu, L. He, *Proc. SPIE* **2016**, 9819, 98191J.
- [264] Z. Tian, R. T. Hinkey, R. Q. Yang, D. Lubyshev, Y. Qiu, J. M. Fastenau, W. K. Liu, M. B. Johnson, *J. Appl. Phys.* **2012**, 111, 024510.
- [265] X. Wang, J. Liu, S. Zhai, F. Liu, Z. Wang, *J. Semicond.* **2014**, 35, 104009.
- [266] M. Hitaka, T. Dougakiuchi, A. Ito, K. Fujita, T. Edamura, *Appl. Phys. Lett.* **2019**, 115, 161102.
- [267] P. Reininger, T. Zederbauer, B. Schwarz, H. Detz, D. MacFarland, A. M. Andrews, W. Schrenk, G. Strasser, *Appl. Phys. Lett.* **2015**, 107, 081107.



Dhafer O. Alshahrani is currently a PhD student in the School of Physics and Astronomy at Cardiff University under the supervision of Dr. Manoj Kesaria. Dhafer has a bachelor's degree in physics from the Physics department, the College of Sciences, King Khalid University (KKU), the Kingdom of Saudi Arabia and a master's degree in physics from the School of Physics and Astronomy, Cardiff University, the UK. His current research interests involve the development of MWIR InAs/GaSb and InAs/InAsSb T2SL photodetectors via optimized fabrication techniques, advanced characterizations, and simulations.



Manoj Kesaria received the PhD degree in 2012 from Jawaharlal Nehru Centre for Advanced Scientific Research (JNCASR), Bangalore, India. Between 2012 and 2018, he has worked as a research scientist and senior research associate at the Universities of Houston, Lancaster, and Sheffield. He is currently a lecturer/assistant professor at the School of Physics and Astronomy at Cardiff University (CU). He is presently involved in the development of novel III-V (nitride, arsenide, and antimonides) compound semiconductor epitaxy, design, simulation, fabrication, and characterization of infrared (SWIR to LWIR), detectors, light-emitting diodes (LED), and thermophotovoltaics (TPV).



Anyebe, Ezekiel Anyebe is a post-doctoral research associate at the school of Engineering, Cardiff University, the UK. He obtained his doctorate in physics (quantum nanotechnology) from Lancaster University, the UK in 2015. He received his master's degree in engineering physics from the Federal University of Agriculture, Makurdi, Nigeria in 2009 and bachelor's degree in physics from the University of Maiduguri, Borno state, Nigeria in 2002.



Diana L. Huffaker (FIEEE, FOSA, FLSW) was the Welsh government Sêr Cymru chair in Advanced Materials and Engineering. She was science director for the Institute for Compound Semiconductors (ICS). Since August 2020, she is a chair of the Electrical Engineering Department at the University of Texas at Arlington. She is a pioneer in MBE growth of III-Sb bulk and quantum dot materials. Her research expertise includes novel III-As and Sb epitaxial methods, fabrication, and high-performance detectors.